

Flexible communication between cell assemblies and ‘reader’ neurons

Céline J. Boucly,^{1,*} Marco N. Pompili,^{1,2*} Ralitsa Todorova,^{1,*}
Eulalie M. Leroux,¹ Sidney I. Wiener,¹ & Michaël Zugaro¹

¹Center for Interdisciplinary Research in Biology (CIRB),

Collège de France, CNRS, INSERM, Université PSL, Paris, France

²Institut de Psychiatrie et Neurosciences de Paris (IPNP),

INSERM, GHU Psychiatrie Neurosciences, Université de Paris, Paris, France

* These authors contributed equally to this work.

Correspondence should be addressed to M.N.P. (marco.pompili@college-de-france.fr)

or M.Z. (michael.zugaro@college-de-france.fr)

Cell assemblies are considered fundamental units of brain activity, underlying diverse functions ranging from perception to memory and decision-making. Cell assemblies have historically been theorized as internal representations of specific stimuli or actions. Alternatively, cell assemblies can be defined without reference to an external world, by their endogenous ability to effectively elicit specific responses in downstream (‘reader’) neurons. However, this compelling framework currently lacks experimental support. Here, we provide evidence for assembly–reader communication. Reader activation was genuinely collective, functionally selective, yet flexible, implementing both pattern separation and completion. These processes occurred at the time scale of membrane integration, synaptic plasticity and gamma oscillations. Finally, assembly–reader couplings were selectively modified upon associative learning, indicating that they were plastic and could become bound to behaviorally relevant variables. These results support cell assemblies as an endogenous mechanism for brain function.

An increasingly influential hypothesis in neuroscience posits that ‘cell assemblies’ are computational units of the brain that can mediate complex information processing beyond the aggregate power of single cells (1–10). Cell assemblies have often been conceived of in relation to external stimuli or motor activity (a ‘representational’ framework), with the underlying assumption that assembly members can code for complementary features that become bound through synchronous activation (11–13). However, this theoretical framework cannot be readily extended to higher order cortical areas, where assemblies (10, 14–19) cannot be assessed in terms of known sensory or motor correlates, and where represented entities are ill defined and notoriously difficult to test. More fundamentally, epistemological arguments (20, 21) suggest that even features that experimenters tentatively assign to assembly members (such as color and shape) may not be purely objective characteristics of external items, but may at least in part result from endogenous properties of the brain itself. Accordingly, seeking objective features represented in cell assemblies could constitute a circular problem. An alternative approach to study cell assemblies is by focusing on brain processes, and considering the effects of assemblies on downstream ‘reader’ neurons. In this ‘reader-centric’ framework (22), a cell assembly can be characterized by its ability to trigger a specific response in one or more target neurons, underlying specific autonomic, behavioral or cognitive functions. However, whether this appealing definition is supported by physiological evidence remains an open question, possibly because of technological limitations even in state-of-the-art causal technologies. Indeed, current approaches, including timed and targeted optogenetics, do not yet permit selective and thorough manipulation of defined groups of neurons at the precise moment when they are about to form specific cell assemblies, but not when they fire individually.

An alternative approach to test this conceptual framework is to identify putative cell assemblies and downstream ‘reader’ neurons during endogenous (non-representational) brain activity, and then show that learning and memory results in selective and predictable changes in assembly–reader relations. For

41 this, we recorded from large neuronal ensembles in two reciprocally interconnected associative brain ar-
42 eas, namely the cortico-amygdalar circuit (Fig. 1a) (23). We first examined collective neural dynamics
43 during sleep, when brain activity is dominated by endogenous processes and is not directly representa-
44 tional. Cell assemblies were identified using a PCA-ICA algorithm (24) (see Methods). Note that this
45 identification method only relies on spike train statistics, but does not require attribution of additional
46 functional properties posited by the respective conceptual frameworks, i.e. feature coding or effective
47 spike transmission. In each sleep session, groups of prefrontal units recurrently fired with high synchrony,
48 forming cell assemblies (15–18) (Fig. 1b,c, median $n = 18$; Fig. S1a,c–e). As expected, cells participating
49 in assemblies (‘members’) fired more synchronously with each other than with non-members, and their
50 spike trains could be reliably predicted from those of other members of the same assembly (‘peer predic-
51 tion’, (14); Fig. 1b). While cell assemblies have been primarily studied in cortical areas (see e.g. (25)),
52 synchronous activity patterns have been reported in subcortical structures (10, 26–28). We thus tested
53 and confirmed (29) that amygdalar neurons also formed cell assemblies (Fig. 1b,d, Fig. S1b–e). Similar to
54 the prefrontal cortex, synchrony and peer prediction were significantly greater than expected by chance.
55 This is consistent with the notion that cell assemblies are a general brain mechanism extending beyond
56 cortical areas (10, 26, 28).

57 According to the ‘reader-centric’ framework, assemblies should effectively elicit discharges in downstream
58 reader neurons. This has two implications: first, activation of an assembly should precede that of its
59 reader within a brief time window, occurring more frequently than expected by chance; and second, this
60 relationship should be dependent on the *collective* activation of the assembly.

61 We first investigated whether cell assemblies reliably triggered spiking in downstream neurons. We sought
62 occurrences of prefrontal assembly activations closely followed (10–30 ms, (30)) by spiking in single
63 amygdalar neurons. In 347 candidate assembly–reader pairs (Fig. 1e,f) this temporal coordination was
64 greater than expected by chance ($p < 0.05$, Monte-Carlo bootstrap). Conversely, in 502 cases, amygdalar
65 assembly activations were consistently followed by prefrontal spikes ($p < 0.05$, Monte-Carlo bootstrap;
66 Fig. 1e,f; see also Fig. S2). Downstream neurons were more likely to discharge when increasing numbers
67 of members were active together (Fig. S3), consistent with the hypothesis that it is the synchronous
68 activation of a cell assembly that drives responses in reader neurons.

69 Second, to assess whether spiking in downstream neurons was actually selective for the collective activa-
70 tion of upstream assemblies, we sought to rule out two confounding scenarios: 1) downstream neurons
71 could be merely responding to each of the assembly members independently, and 2) they could be respond-
72 ing to the compound activation of the assembly (excitatory drive), irrespective of the precise identity of
73 participating members.

74 We first verified that assembly members exerted a synergistic, rather than independent (linearly sum-
75 mating), influence on their targets. In one extreme scenario, one or two ‘vocal’ members might suffice to
76 evoke maximal discharge in the target neuron while the other members would not have any impact on the
77 response. To rule out this possibility, we discarded all assembly activations in which the most effective
78 members were active. In the remaining cases, the responses of the target neurons remained well above
79 their baseline firing rates (Fig. 2a; Fig. S4). To further address this scenario in its most general form,
80 we trained a generalized linear model (GLM) to predict reader activity from the spikes of the respective
81 assembly members outside assembly activation epochs. We then used this pre-trained GLM to predict
82 responses to assembly activations. This estimated how the reader would respond if it were processing each
83 of its inputs independently. The observed response to assembly activations exceeded this linear estimate
84 and peaked at a delay of ~ 20 ms (Fig. 2b; Fig. S5), indicating that the collective activation of assembly
85 members was capable of evoking greater responses than the sum of their individual contributions.

86 We then assessed whether members were interchangeable, or even dispensable, provided their total spike
87 count remained the same. To test for this, for any given pair of assembly members (A and B), we compared
88 reader responses when each of the two members emitted exactly one spike (AB) vs when only one of the
89 two members emitted exactly two spikes (AA), thus maintaining a constant number of assembly spikes
90 while blurring cell identity. This analysis revealed that the identity of participating members mattered
91 beyond their compound activity (Fig. 2c, Fig. S6). This is consistent with the hypothesis that the response
92 of the reader neuron should depend on detailed spatio-temporal properties of its inputs (e.g. precisely
93 timed spike patterns impinging on specific combinations of dendritic branches (31)).

94 These results are consistent with the prediction that assemblies exert a collective impact on their readers.
95 To investigate the time scale of this synergistic effect, we repeated these analyses for varying interspike

96 intervals and assembly durations. Both approaches yielded results consistent with an endogenous time
97 scale of up to ~ 20 -25 ms for effective cell assemblies (Fig. 2c, Fig. S7, and Fig. S8). This time scale corre-
98 sponds to those of functionally relevant cellular and network properties, including membrane integration
99 time constants and local delays (32), optimal time windows for spike timing dependent potentiation of
100 synaptic efficacy (33), and the period of synchronizing gamma oscillations (34).

101 Note that a given assembly could drive multiple reader neurons which may very well, in turn, participate
102 in cell assemblies. Indeed, in the amygdala 82 readers (out of 204) did participate in 147 assemblies, 42 of
103 which were detected by prefrontal readers. Further, compared to other amygdalar neurons, amygdalar
104 readers were significantly more likely to participate in cell assemblies targeting prefrontal readers ($p=1.2e$ -
105 4, chi-square test). Similarly, 278 (out of 404) prefrontal readers participated in 247 assemblies, 104 of
106 which triggered amygdalar readers, and thus were significantly more likely than other prefrontal neurons
107 to target amygdalar readers ($p=2.6e-21$, chi-square test). This is consistent with the notion that cell
108 assemblies can be detected by cell assemblies, extending the concept of reader neurons and providing a
109 generalized mechanism for bidirectional communication.

110 We next investigated computational and functional properties of the assembly-reader mechanism. Does
111 assembly reading manifest pattern completion (similar reader responses upon activation of a sufficient
112 subset of assembly members) and pattern separation (discrimination between partially overlapping as-
113 semblies)? To test for pattern completion, we assessed reader responses following partial activation of
114 upstream assemblies, and measured how they increased with the number of active members. Reader
115 responses did not simply increase proportionally to the number of active members but were significantly
116 better fit by a sigmoid curve, thus providing evidence for pattern completion (35) (Fig. 3a, Fig. S9).
117 Regarding pattern separation, we first compared the activity of readers following activation of each of
118 the simultaneously recorded assemblies, and confirmed that reader responses were highly selective for
119 specific assemblies (Fig. 3b, Fig. S10). We then focused on cell assemblies with multiple ($\geq 25\%$) common
120 members, and found that reader neurons effectively discriminated between such overlapping assemblies,
121 providing further evidence for pattern separation (Fig. 3c, Fig. S11). Thus, the assembly-reader mecha-
122 nism is both robust and selective, since it can implement both pattern completion and pattern separation.

123 Having identified assembly-reader pairs and found evidence for two of their widely posited computational
124 properties, namely pattern separation and completion, we set out to test the prediction that their relation
125 should be altered by learning and memory in a selective and predictable manner. We compared assembly-
126 reader pairs before and after a standard fear conditioning and extinction protocol known to recruit the
127 prefronto-amygdalar circuit (36-39) (Fig. 4a; see Methods). During fear conditioning and subsequent
128 sleep, fear-related signals would be expected to flow from the amygdala to the prefrontal cortex (40).
129 We thus examined prefrontal reader responses to amygdalar assemblies, and compared activity during
130 sleep preceding vs following training, when reactivation of cell assemblies has been shown to mediate
131 memory consolidation (16, 19, 41). We found numerous examples of amygdalar cell assemblies that were
132 active in both sleep sessions, but formed novel associations with downstream prefrontal neurons following
133 fear conditioning (Fig. 4a). Other downstream prefrontal neurons no longer responded significantly to
134 amygdalar cell assemblies in post-conditioning sleep (Fig. 4a).

135 To confirm that these changes were specifically related to fear learning as opposed to e.g. exploratory
136 activity, we compared them to changes before and after a control session where no fearful stimuli were
137 provided. Fear conditioning was followed by significantly greater responses in prefrontal readers to amyg-
138 dalar assemblies (Fig. 4b). Further, in contrast to fear conditioning, fear extinction did not result in such
139 changes (Fig. 4a), indicating that variations in assembly-reader relations were not broadly elicited by
140 general fearful behavior, but rather reflected the specific process of forming new fear memories.

141 Conversely, during fear extinction, the prefrontal cortex would be expected to alter amygdalar signals
142 (30). Consistent with this, the relation between prefrontal assemblies and amygdalar readers underwent
143 substantial reorganization following fear extinction (Fig. 4c). Again, this was specific to this particular
144 cognitive process, since fear conditioning did not yield changes in assembly-reader pairs significantly
145 different from control sessions (Fig. 4b).

146 Our results indicate that single neurons in downstream structures can reliably and selectively respond
147 to the activation of upstream cell assemblies. The responses were stronger than expected for the sum of
148 independent inputs, and depended on the identity of the participating neurons rather than their aggregate
149 drive. The process therefore implemented a genuinely collective computation, and supports a possible
150 alternative, operational, rather than representational, definition for cell assemblies (22), without reference

151 to features of external stimuli or actions (8). Individual neurons could be involved in both cell assembly
152 and reader functions, suggesting that the readout of cell assemblies was not only performed by isolated
153 neurons, but more generally by other cell assemblies as well (42, 43), which would then communicate
154 with cell assemblies in other areas. In addition, because a fraction of the members were sufficient to
155 elicit reader responses, yet readers discriminated between partly overlapping assemblies, the process
156 implemented both pattern separation and pattern completion (1, 44). Finally, flexible functional changes
157 in assembly–reader pairing emerged during learning. Using fear conditioning and extinction as a model,
158 we showed that assembly–reader relations selectively changed during learning in a behaviorally-relevant
159 manner, supporting the role of cell assemblies as functional units of brain computation.

160 Acknowledgments

161 We thank G. Makdah for help with data acquisition and Y. Dupraz for technical support. This project
162 was funded by the Agence Nationale de la Recherche (ANR-17-CE37-0016-01) (M.Z.), Fondation pour
163 la Recherche Médicale (Équipe FRM EQU202103012768) (M.Z.), Labex MemoLife (ANR-10-LABX-54
164 MEMO LIFE, ANR-10-IDEX-0001-02 PSL*) (M.N.P. and S.I.W.), French Ministry of Research (C.B.),
165 and Collège de France (R.T.) The authors declare no competing interests. Research design: C.J.B.,
166 M.N.P., R.T., S.I.W., M.Z. Experiments: E.M.L., M.N.P. Data analysis design: C.J.B., M.N.P., R.T.,
167 S.I.W., M.Z. Data analysis: C.B.J., R.T. Manuscript: C.B.J., M.N.P., R.T., S.I.W., M.Z.

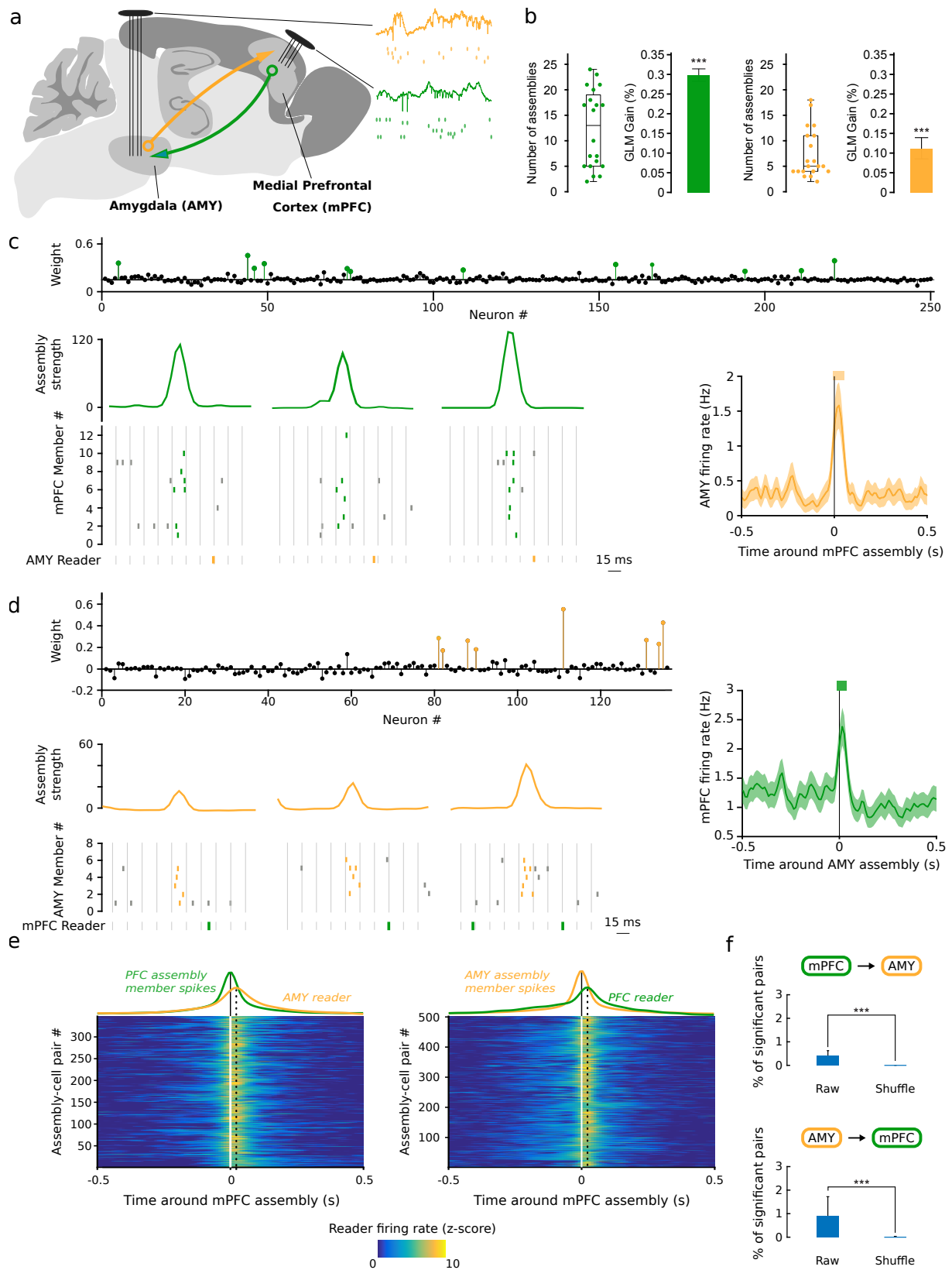


Fig. 1. Cell assembly activations are closely followed by downstream spiking. **a**, Simultaneous high-density recordings in the bi-directionally connected medial prefrontal cortex and amygdala ($n = 4$ rats; 5 sessions each). **b**, Numbers of assemblies in prefrontal (left, median $n = 13$) and amygdalar (right, median $n = 5$) recordings in individual sessions (boxes and whiskers: distribution quartiles). Median \pm s.e.m. peer prediction of the activity of assembly members from other members (gain relative to shuffled data, *** $p < 0.001$; Wilcoxon rank sum test). *continued* \rightarrow

Fig. 1 (continued). **c**, Example medial prefrontal cortical assembly activations closely (10–30 ms) followed by significant responses of an amygdalar neuron. Top: cell assembly weights (colored circles: assembly members, black circles: non-members). Bottom left: examples of assembly activation (curves: activation strength) followed by downstream spiking (rasters: prefrontal spikes within (green) and outside (gray) epochs of assembly activation; orange rasters: amygdalar spikes). Right: firing rate of amygdalar neuron centered on all prefrontal assembly activations (mean \pm s.e.m.). Thick orange horizontal bar indicates significant responses ($p < 0.05$: Monte-Carlo bootstrap test; see Methods). **d**, Same as (c) for amygdalar assembly and downstream prefrontal neuron. **e**, Average downstream responses (z-scored firing rates) centered on assembly activations, over all significant pairs (color plots), and averaged across pairs (color curves) compared with the average activity of the upstream assembly. Left: prefrontal assemblies and amygdalar downstream neurons. Right: amygdalar assemblies and downstream prefrontal neurons. **f**, Percentage of significant assembly-reader pairs found in shuffled recordings vs. real data (** $p < 0.001$, Wilcoxon signed-rank test).

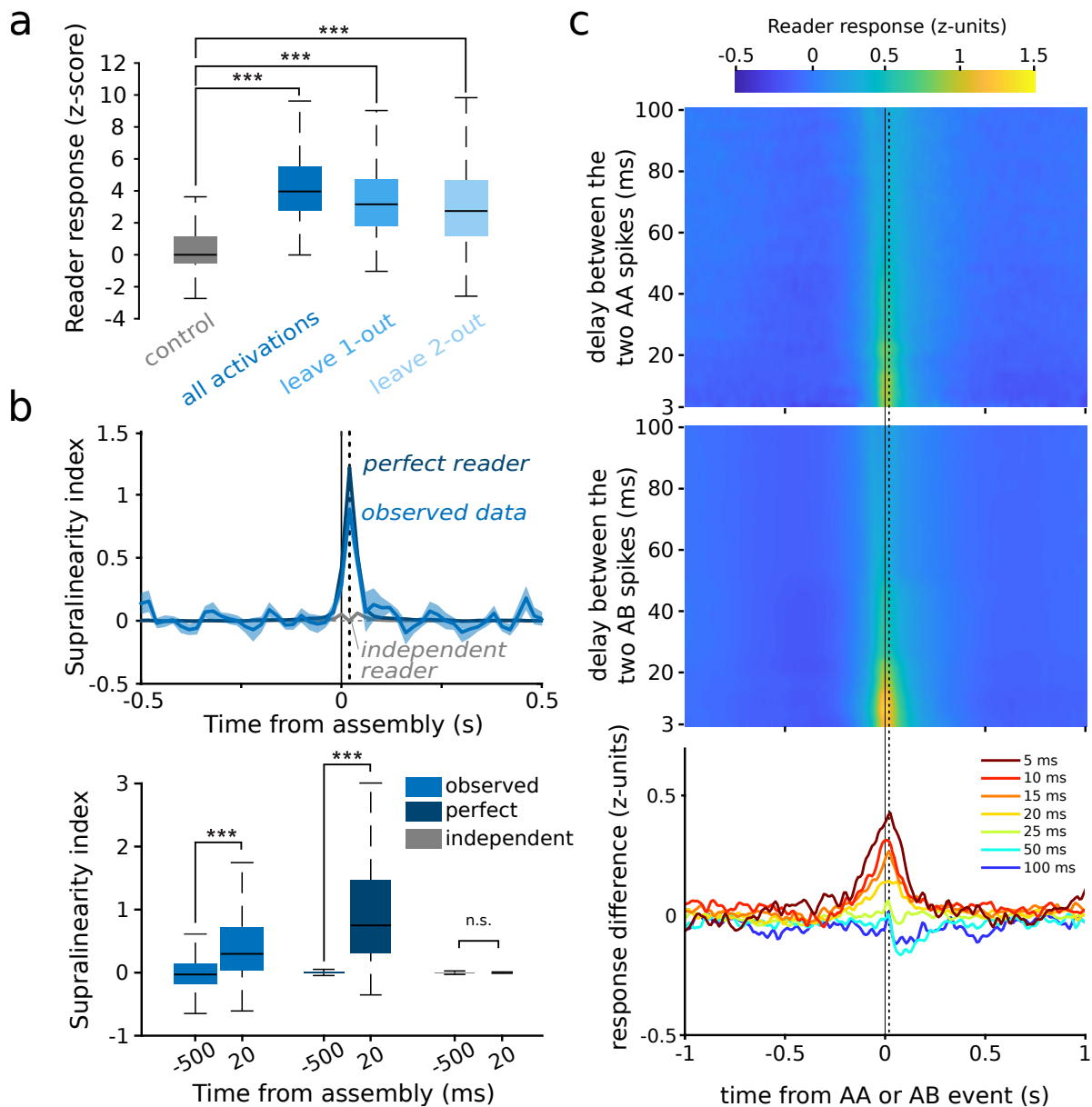


Fig. 2. Readers respond to the collective activity of assemblies. **a**, Average response of reader neurons to upstream assembly activations when the most effective members of upstream assemblies were not recruited. As a control, assemblies and downstream neurons were taken randomly among non-significant pairs. **b**, Supralinearity of reader responses to the collective activity of assembly members. Top: Supralinearity index of data (blue curve) compared to a simulated perfect collective reader (dark blue curve) and to a simulated independent reader (gray curve). Bottom: Supralinearity index 20 ms after assembly activations was significantly greater than at baseline (500 ms prior to assembly activations) for both the observed data ($***p < 0.001$, Wilcoxon signed-rank test) and the simulated perfect collective readers ($***p < 0.001$, Wilcoxon signed-rank test), but not for the simulated independent readers ($p=0.7916$, Wilcoxon signed-rank test). **c**, Top: mean z-scored responses of reader neurons to two successive spikes of the same member (AA) of an upstream assembly as a function of the temporal delay between the two spikes. Center: same as top, but for reader responses to two successive spikes of two different assembly members (AB). Bottom: difference between the two (AB–AA), for varying temporal delays. The response to co-activations of different members (AB) is greater than the response to multiple activations of the same member (AA) only for brief (<25 ms) delays between spikes ($***p < 0.001$, Wilcoxon signed-rank test). Vertical dashed lines indicate 20 ms.

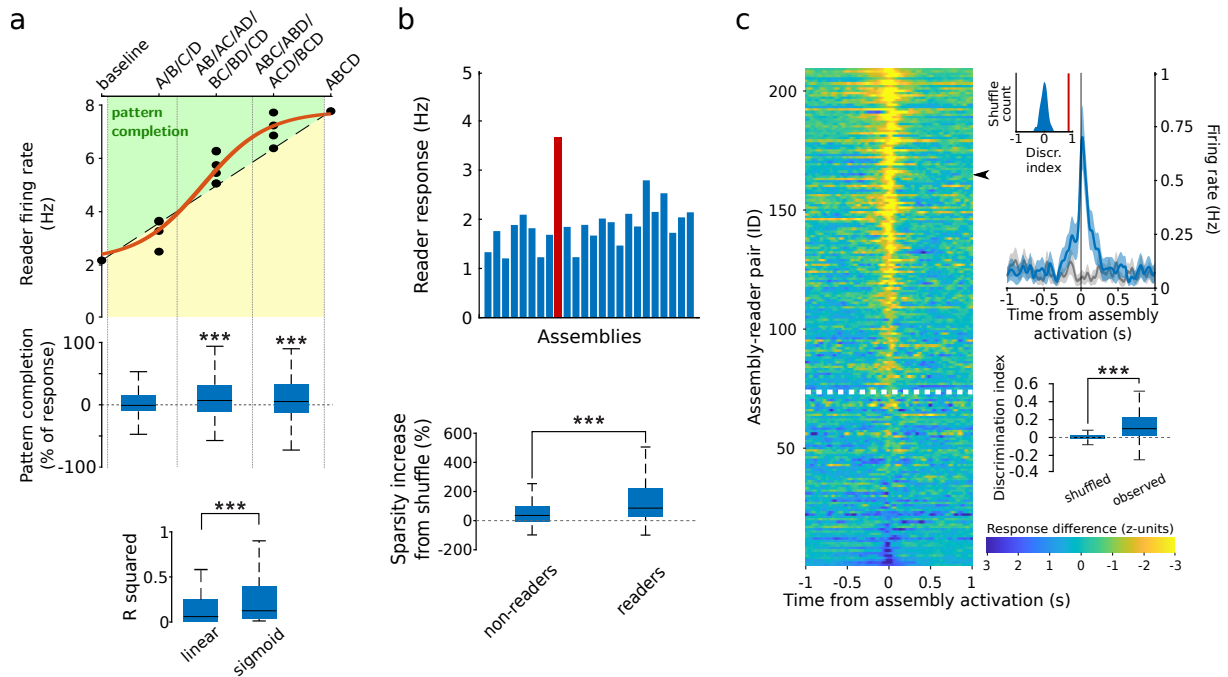


Fig. 3. Computational properties of the assembly–reader mechanism. **a**, Pattern completion. Response of one example reader to incomplete activations of a 4-member assembly (ABCD). Dashed line: proportional response. Red curve: best-fit sigmoid. Green zone: pattern completion. Center: boost in reader response (relative to a proportional response) for all assembly–reader pairs as a function of the number of active assembly members. The gain was significant for the second and third quantiles ($***p < 0.001$, Wilcoxon signed-rank test). Bottom: Proportional vs sigmoidal fits of observed data ($***p < 0.001$, Wilcoxon signed-rank test). **b**, Pattern separation. Top: responses of an example reader neuron to each cell assembly detected in the same session (red bar: specific assembly read by this downstream neuron). Bottom: sparsity (increase relative to shuffled data) of the responses of reader neurons to assembly activations was significantly greater than shuffled data ($p < 0.001$, Wilcoxon signed rank test) and than responses of non-reader neurons ($***p < 0.001$, Wilcoxon rank sum test). **c**, Pattern separation. Left: Mean difference between reader responses to activations of paired assemblies and other assemblies with overlapping members ($\geq 25\%$ of all members). Data are sorted by discrimination index. Responses above the white dotted line displayed significant pattern separation (discrimination index greater than 95% of the shuffled data). Top right: response of an example reader (black arrow) to its paired assembly (blue curve) vs to another assembly with overlapping members (gray curve) (mean \pm s.e.m.). Bottom right: Observed discrimination indices were greater than the discrimination indices for shuffled data ($***p < 0.001$, Wilcoxon rank sum test).

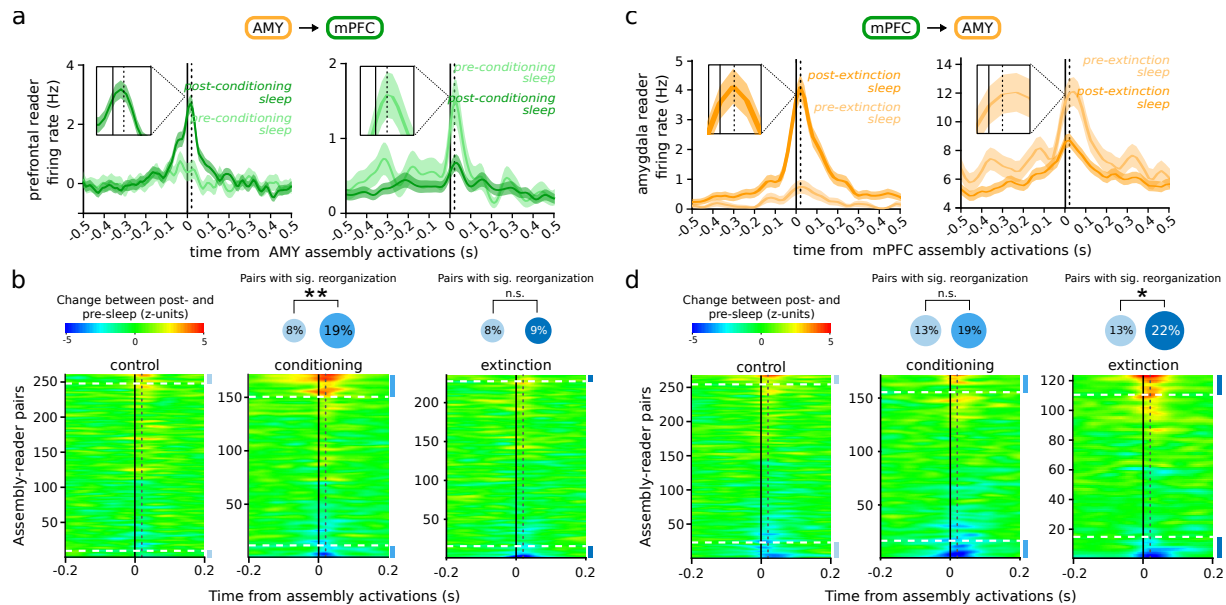


Fig. 4. Learning-related changes in assembly–reader relations. **a**, Examples of a reader increasing (left) or decreasing (right) their responses (shaded area: mean \pm s.e.m.) to assembly activations before (light green) and after (green) fear conditioning. Dotted line: 20 ms. **b**, Left: Responses of a prefrontal reader between post and pre sleep, centered on amygdalar assembly activations. Data are sorted according to response magnitudes. Assembly–reader pairs above the higher dashed line (resp. below the lower dashed line) significantly ($p < 0.05$, Monte-Carlo bootstrap test) increased (resp. decreased) their responses in post-task sleep. A greater proportion of assembly–reader pairs significantly changed their responses ($p < 0.05$, Monte-Carlo bootstrap test) following fear conditioning than following control sessions (blue bars and disks; $**p = 0.0017$, chi-square test). On the contrary, the number of assembly–reader pairs that significantly changed their responses was not greater after fear extinction than after control sessions ($p > 0.05$, chi-square test). **c**, Left: Same as **(a)** for example amygdalar reader responses to prefrontal assemblies following fear extinction. **d**, Left: Same as **(b)** for amygdalar reader responses to prefrontal assemblies following control sessions vs fear extinction sessions. A greater proportion of assembly–reader pairs significantly changed their response ($p < 0.05$, Monte-Carlo bootstrap test) after fear extinction than after control sessions (blue bars and disks; $*p = 0.0347$, chi-square test). On the contrary, the number of assembly–reader pairs that significantly changed their responses was not greater after fear conditioning than after control sessions ($p > 0.05$, chi-square test).

References

- 168 1. D. O. Hebb. *The Organization of Behavior*. Wiley, 1949.
- 169 2. H. B. Barlow. Single units and sensation: A neuron doctrine for perceptual psychology? *Perception*,
170 1(4):371–394, 1972.
- 171 3. V. Braitenberg. Cell Assemblies in the Cerebral Cortex. In *Theoretical Approaches to Complex*
172 *Systems*, pages 171–188. Springer, Berlin, Heidelberg, 1978.
- 173 4. J. J. Hopfield. Neural networks and physical systems with emergent collective computational abilities.
174 *PNAS*, 79(8):2554–2558, 4 1982.
- 175 5. A. Pouget, P. Dayan, and R. Zemel. Information processing with population codes. *Nature Reviews*
176 *Neuroscience*, 1(2):125–132, 2000.
- 177 6. F. Varela, J. P. Lachaux, E. Rodriguez, and J. Martinerie. The brainweb: Phase synchronization and
178 large-scale integration. *Nature Reviews Neuroscience*, 2(4):229–239, 2001.
- 179 7. K. D. Harris. Neural signatures of cell assembly organization. *Nature Reviews Neuroscience*, 6(5):399–
180 407, 2005.
- 181 8. H. Eichenbaum. Barlow versus Hebb: When is it time to abandon the notion of feature detectors
182 and adopt the cell assembly as the unit of cognition? *Neuroscience Letters*, 680:88–93, 2018.
- 183 9. M. El-Gaby, H. M. Reeve, V. L. dos Santos, N. Campo-Urriza, P. V. Perestenko, A. Morley, L. A. M.
184 Strickland, I. P. Lukács, O. Paulsen, and D. Dupret. An emergent neural coactivity code for dynamic
185 memory. *Nature Neuroscience*, 2021.
- 186 10. V. J. Oberto, C. J. Boucly, H. Gao, R. Todorova, M. Zugaro, and S. I. Wiener. Distributed cell
187 assemblies spanning prefrontal cortex and striatum. *Current Biology*, 32(1):1–13.e6, 2021.
- 188 11. C. von der Malsburg. The correlation theory of brain function. In *Internal Report 81-2*. Dept. of
189 Neurobiology, Max-Planck-Institute for Biophysical Chemistry, Göttingen, Germany, 1981.
- 190 12. A. P. Georgopoulos, A. B. Schwartz, and R. E. Kettner. Neuronal population coding of movement
191 direction. *Science*, 233(4771):1416 – 1419, 1986.
- 192 13. C. M. Gray, P. König, A. K. Engel, and W. Singer. Oscillatory responses in cat visual cortex exhibit
193 inter-columnar synchronization which reflects global stimulus properties. *Nature*, 338(6213):334 –
194 337, 1989.
- 195 14. K. D. Harris, J. Csicsvari, H. Hirase, G. Dragoi, and G. Buzsáki. Organization of cell assemblies in
196 the hippocampus. *Nature*, 424(6948):552–556, 7 2003.
- 197 15. S. Fujisawa, A. Amarasingham, M. T. Harrison, and G. Buzsáki. Behavior-dependent short-term
198 assembly dynamics in the medial prefrontal cortex. *Nature Neuroscience*, 11(7):823–833, 7 2008.
- 199 16. A. Peyrache, M. Khamassi, K. Benchenane, S. I. Wiener, and F. P. Battaglia. Replay of rule-learning
200 related neural patterns in the prefrontal cortex during sleep. *Nature Neuroscience*, 12(7):919–926,
201 2009.
- 202 17. K. Benchenane, A. Peyrache, M. Khamassi, P. L. Tierney, Y. Gioanni, F. P. Battaglia, and S. I.
203 Wiener. Coherent theta oscillations and reorganization of spike timing in the hippocampal-prefrontal
204 network upon learning. *Neuron*, 66(6):921–936, 6 2010.
- 205 18. C. Dejean, J. Courtin, N. Karalis, F. Chaudun, H. Wurtz, T. C. Bienvenu, and C. Herry. Prefrontal
206 neuronal assemblies temporally control fear behaviour. *Nature*, 535(7612):420–424, 7 2016.
- 207 19. R. Todorova and M. Zugaro. Isolated cortical computations during delta waves support memory
208 consolidation. *Science*, 366(6463):377–381, 10 2019.
- 209 20. H. R. Maturana and F. J. Varela. *The tree of knowledge: The biological roots of human understanding*.
210 New Science Library/Shambhala Publications, 1987.
- 211 21. G. Buzsáki. *The brain from inside out*. Oxford University Press, 2019.
- 212

- 213 22. G. Buzsáki. Neural Syntax: Cell Assemblies, Synapsembles, and Readers. *Neuron*, 68(3):362–385, 11
214 2010.
- 215 23. C. J. Reppucci and G. D. Petrovich. Organization of connections between the amygdala, medial
216 prefrontal cortex, and lateral hypothalamus: a single and double retrograde tracing study in rats.
217 *Brain Structure and Function*, 221(6):2937–2962, 7 2016.
- 218 24. V. Lopes dos Santos, S. Ribeiro, and A. B. Tort. Detecting cell assemblies in large neuronal popula-
219 tions. *Journal of Neuroscience Methods*, 220(2):149–166, 11 2013.
- 220 25. K. D. Harris. Cell assemblies of the superficial cortex. *Neuron*, 76(2):263–265, 2012.
- 221 26. C. M. Pennartz, E. Lee, J. Verheul, P. Lipa, C. A. Barnes, and B. L. McNaughton. The ventral
222 striatum in off-line processing: Ensemble reactivation during sleep and modulation by hippocampal
223 ripples. *Journal of Neuroscience*, 24(29):6446–6456, 7 2004.
- 224 27. L. Sjulson, A. Peyrache, A. Cumpelik, D. Cassataro, and G. Buzsáki. Cocaine Place Conditioning
225 Strengthens Location-Specific Hippocampal Coupling to the Nucleus Accumbens. *Neuron*, 98(5):926–
226 934, 6 2018.
- 227 28. H. Miyawaki and K. Mizuseki. De novo inter-regional coactivations of preconfigured local ensembles
228 support memory. *Nature communications*, 13(1):1–21, 2022.
- 229 29. K. M. Gothard. Multidimensional processing in the amygdala. *Nature Reviews Neuroscience*,
230 21(10):565 – 575, 2020.
- 231 30. E. Likhtik, J. G. Pelletier, R. Paz, and D. Paré. Prefrontal control of the amygdala. *Journal of*
232 *Neuroscience*, 25(32):7429 – 7437, 2005.
- 233 31. T. Branco, B. A. Clark, and M. Häusser. Dendritic discrimination of temporal input sequences in
234 cortical neurons. *Science*, 329(5999):1671 – 1675, 2010.
- 235 32. C. Koch, M. Rapp, and I. Segev. A brief history of time (constants). *Cerebral Cortex*, 6(2):93–101,
236 1996.
- 237 33. G. Q. Bi and M. M. Poo. Synaptic modifications in cultured hippocampal neurons: Dependence on
238 spike timing, synaptic strength, and postsynaptic cell type. *Journal of Neuroscience*, 18(24):10464–
239 10472, 12 1998.
- 240 34. G. Buzsáki and E. W. Schomburg. What does gamma coherence tell us about inter-regional neural
241 communication? *Nature Neuroscience*, 18(4):484 – 489, 2015.
- 242 35. J. L. McClelland and N. H. Goddard. Considerations arising from a complementary learning systems
243 perspective on hippocampus and neocortex. *Hippocampus*, 6(6):654 – 665, 1996.
- 244 36. M. A. Morgan and J. E. LeDoux. Differential contribution of dorsal and ventral medial prefrontal cor-
245 tex to the acquisition and extinction of conditioned fear in rats. *Behavioral Neuroscience*, 109(4):681,
246 1995.
- 247 37. J. Muller, K. P. Corodimas, Z. Fridel, and J. E. LeDoux. Functional inactivation of the lateral
248 and basal nuclei of the amygdala by muscimol infusion prevents fear conditioning to an explicit
249 conditioned stimulus and to contextual stimuli. *Behavioral Neuroscience*, 111(4):683–682, 1997.
- 250 38. C. Herry, S. Ciocchi, V. Senn, L. Demmou, C. Müller, and A. Lüthi. Switching on and off fear by
251 distinct neuronal circuits. *Nature*, 454(7204):600–606, 2008.
- 252 39. D. Sierra-Mercado, N. Padilla-Coreano, and G. J. Quirk. Dissociable roles of prelimbic and infral-
253 imbic cortices, ventral hippocampus, and basolateral amygdala in the expression and extinction of
254 conditioned fear. *Neuropsychopharmacology*, 36(2):529–538, 1 2011.
- 255 40. D. Popa, S. Duvarci, A. T. Popescu, C. Léna, and D. Paré. Coherent amygdalocortical theta promotes
256 fear memory consolidation during paradoxical sleep. *PNAS*, 107(14):6516–6519, 2010.
- 257 41. G. Girardeau, I. Inema, and G. Buzsáki. Reactivations of emotional memory in the hippocampus-
258 amygdala system during sleep. *Nature Neuroscience*, 20(11):1634–1642, 2017.
- 259 42. M. Abeles. *Local Cortical Circuits*. Studies of Brain Function. Springer Berlin Heidelberg, 1982.

- 260 43. Y. Ikegaya, G. Aaron, R. Cossart, D. Aronov, I. Lampl, D. Ferster, and R. Yuste. Synfire chains and
261 cortical songs: Temporal modules of cortical activity. *Science*, 304(5670):559 – 564, 2004.
- 262 44. A. Lansner and E. Fransen. Modelling hebbian cell assemblies comprised of cortical neurons. *Network*,
263 3(2):105 – 119, 1992.
- 264 45. M. O. Pasquet, M. Tihy, A. Gourgeon, M. N. Pompili, B. P. Godsil, C. Léna, and G. P. Dugué.
265 Wireless inertial measurement of head kinematics in freely-moving rats. *Scientific Reports*, 6:35689,
266 2016.
- 267 46. M. Pachitariu, N. A. Steinmetz, S. N. Kadir, M. Carandini, and K. D. Harris. Fast and accurate spike
268 sorting of high-channel count probes with kilosort. In D. Lee, M. Sugiyama, U. Luxburg, I. Guyon,
269 and R. Garnett, editors, *Advances in Neural Information Processing Systems*, volume 29. Curran
270 Associates, Inc., 2016.
- 271 47. L. Hazan, M. Zugaro, and G. Buzsáki. Klusters, NeuroScope, NDManager: A free software suite for
272 neurophysiological data processing and visualization. *Journal of Neuroscience Methods*, 155(2):207–
273 216, 2006.
- 274 48. M. N. Pompili and R. Todorova. Discriminating sleep from freezing with cortical spindle oscillations.
275 *Frontiers in Neural Circuits*, 16, 2022.
- 276 49. G. Paxinos and C. Watson. *The Rat Brain in Stereotaxic Coordinates*. Academic Press, 2013.
- 277 50. V. A. Marčenko and L. A. Pastur. Distribution of eigenvalues for some sets fo random matrices.
278 *Mathematics of the USSR-Sbornik*, 1(4):457–483, 4 1967.
- 279 51. N. Otsu. Threshold selection method from gray-level histograms. *IEEE Transactions on Systems,*
280 *Man, and Cybernetics*, SMC-9(1):62–66, 1979.
- 281 52. G. Rothschild, E. Eban, and L. M. Frank. A cortical-hippocampal-cortical loop of information
282 processing during memory consolidation. *Nature Neuroscience*, 20(2):251–259, 2 2017.

283 Animals

284 Four male Long-Evans rats (350–400 g at the time of surgery) were housed individually in monitored
285 conditions (21°C and 45% humidity) and maintained on a 12h light – 12h dark cycle. In order to avoid
286 obesity, food was restricted to 13–16 g of rat chow per day, while water was available *ad libitum*. To
287 habituate the rats to human manipulation, they were handled each workday. All experiments conformed
288 to the approved protocols and regulations of the local ethics committee (Comité d'éthique en matière
289 d'expérimentation animale Paris Centre et Sud n°59), the French Ministries of Agriculture, and Research.

290 Surgery

291 The rats were deeply anesthetized with ketamine-xylazine (Imalgene 180 mg/kg and Rompun 10 mg/kg)
292 and anesthesia was maintained with isoflurane (0.1-1.5% in oxygen). Analgesia was provided by subcu-
293 taneous injection of buprenorphine (Buprecaire, 0.025 mg/kg) and meloxicam (Metacam, 3 mg/kg). The
294 animals were implanted with a custom built microdrive (144–252 channels) carrying 24, 32, or 42 inde-
295 pendently movable hexatrodes (bundles of 6 twisted tungsten wires, 12 µm in diameter, gold-plated to
296 ~200 kΩ). The electrode tips were typically implanted 0.5 mm above the (bilateral) target brain regions.
297 Miniature stainless steel screws were implanted above the cerebellum to serve as electrical reference and
298 ground.

299 During recovery from surgery (minimum 7 days), the rats received antibiotic (Marbofloxacin, 2 mg/kg)
300 and analgesic (Meloxicam, 3 mg/kg) treatments via subcutaneous injections and were provided with food
301 and water *ad libitum*. The recording electrodes were then progressively lowered until they reached their
302 targets and adjusted to optimize yield and stability.

303 Data acquisition and processing

304 Brain activity was recorded using a 256-channel digital data acquisition system (KJE-1001, Amplipex,
305 Szeged, Hungary). The signals were acquired with four 64-channel headstages (Amplipex HS2) and
306 sampled wideband at 20,000 Hz. An inertial measurement unit (IMU, custom-made non-wireless version
307 of the one described in (45)) sampled the 3D angular velocity and linear acceleration of the head at 300 Hz.
308 To determine the instantaneous position of the animal, a red LED mounted on the headstage was imaged
309 by overhead webcams at 30 Hz. Animal behavior was also recorded at 50 Hz by lateral video cameras
310 (acA25000, Basler). Off-line spike sorting was performed using KiloSort (46) for prefrontal units, and
311 KlustaKwik (K.D. Harris, <http://klustakwik.sourceforge.net>) for amygdalar units. The resulting
312 clusters were visually inspected using Klusters (47) to reject noise and to merge erroneously split units.
313 Neurophysiological and behavioral data were explored using NeuroScope (47). LFPs were derived from
314 wideband signals by downsampling all channels to 1250 Hz.

315 **Scoring of behavioral and brain states** Automatic detection of immobility was performed by thresh-
316 olding the angular speed calculated from gyroscopic data as described in (45). LFP data was visualized
317 using Neuroscope (47) and slow-wave sleep (SWS) was detected as previously described (48).

318 **Histological identification of recording sites** At the end of the experiments, recording sites were
319 marked with small electrolytic lesions (~20 µA for 20 s, one lesion per bundle). After a delay of at least
320 three days to permit glial scarring, rats were deeply anesthetized with a lethal dose of pentobarbital, and
321 intracardially perfused with saline (0.9%) followed by paraformaldehyde (4%). Coronal slices (35 µm)
322 were stained with cresyl-violet and imaged with conventional transmission light microscopy. Recording
323 sites were reconstructed by comparing the images with the stereotaxic atlas of (49).

324 Data analysis and statistics

325 Data were analyzed in Matlab (MathWorks, Natick, MA) using the Freely Moving Animal Toolbox
326 (M. Zugaro and R. Todorova, <http://fmatoolbox.sourceforge.net>) and custom written programs. De-
327 tailed statistics are reported in Table S1.

328 Identification of cell assemblies

329 A standard unsupervised method based on principal and independent component analyses (PCA (16) and
330 ICA (24)) detected the co-activation of simultaneously recorded neurons. Spike trains recorded during
331 SWS were first binned into 15-ms bins and z-scored to generate a z-scored spike count matrix Z , where
332 $Z_{i,j}$ represents the activity of neuron i during time bin j . Principal components (PCs) were computed
333 by eigen decomposition of the correlation matrix of Z . Principal components associated with eigenvalues
334 exceeding the upper bound of the Marčenko-Pastur distribution were considered significant (50). We
335 then carried out ICA (using the fastICA algorithm by H. Gävert, J. Hurri, J. Särelä, and A. Hyvärinen,
336 <http://research.ics.aalto.fi/ica/fastica>) on the projection of Z onto the subspace spanned by
337 significant PCs. Independent component (IC) weights were scaled to unit length and by convention the
338 arbitrary signs of the weights were set so that the highest absolute weight was positive. Members of
339 cell assemblies were identified using Otsu’s method (51) to divide the absolute weights into two groups
340 maximizing inter-class variance, and neurons in the group with greater absolute weights were classified
341 as members. Goodness of separation was quantified using Otsu’s effectiveness metric, namely the ratio
342 of the inter-class variance to the total variance. This procedure yielded a set of vectors C_i representing
343 the detected cell assemblies.

344 In theory, it is possible to observe an assembly with both positive and negative weight members (‘mixed-
345 signs’ assemblies), representing two groups of anti-correlated neurons that inhibit each other. However,
346 in our dataset mixed-signs assemblies were composed of more numerous members with lower separation
347 quality compared to same-sign assemblies (Fig. S12), suggesting that mixed-signs assemblies may result
348 from limitations of the ICA method to identify independent components from the PCs (24). We therefore
349 discarded mixed-signs assemblies from further analyses.

350 Peer prediction

351 Population coupling of assembly members was verified by quantifying to what extent the spiking activity
352 of one member could be predicted from the spiking activity of all other members (14). For cross-validation,
353 spike trains were divided into two non-overlapping partitions. Using one partition (‘training set’), for
354 each assembly member i , a generalized linear model (GLM) was trained to predict its activity Z_i from
355 the activity of all other members of the same assembly. To test performance, the GLM prediction
356 error was computed on the remaining partition (‘test set’). This procedure was repeated exchanging
357 the training and testing sets, resulting in two-fold cross-validation. The quality of the prediction was
358 assessed by comparing the median prediction error e to the median error $e_{shuffled}$ obtained by shuffling
359 50 times the predictions relative to the observed activity Z_i . The prediction gain g was defined as
360 $g = e_{shuffled}/e - 1$ (52).

361 Assembly activations

To study downstream responses to assemblies, we computed an instantaneous assembly activation strength:

$$A_i(t) = z_i(t)^T \cdot f(C_i^T \cdot C_i) \cdot z_i(t)$$

362 where C_i contains the weights of the members of the i^{th} assembly, and $z_i(t)$ is the activity of the assembly
363 members at time t (computed using 15-ms windows and a 1-ms sliding window), and $f(C_i^T \cdot C_i)$ is a
364 transformation of the outer product where the diagonal is set to 0, so that spiking in a single neuron
365 does not contribute a high activation strength. Note that only the activity of assembly members were
366 used in this computation to ensure that the activation strength reflects periods of coactivity of the
367 assembly members rather than global fluctuations in the activity of cells with low weights (see Fig. S13).
368 Assemblies were considered to be active when their activation strength exceeded a threshold of the 95th
369 percentile of the values above baseline (the median, corresponding to empty bins). The midpoint of each
370 threshold-exceeding activation was taken as assembly activation peak for further analyses.

371 Downstream responses to cell assemblies

372 For each candidate reader cell i , we computed the peri-event time histogram (PETH) of its spikes in
373 the 2 s interval (10 ms bins) centered on assembly activation peaks. PETHs with fewer than 30 spikes
374 were discarded. To make computations tractable, candidate assembly–reader pairs were pre-selected
375 for further analyses if the z-scored response exceeded 2SDs in the 10–30 ms window following assembly
376 activations (corresponding to the \sim 20-ms conduction delay between these structures (30)). For each
377 candidate assembly–reader pair, the response matrix was shuffled 200 times to determine pointwise and
378 global confidence intervals (15). The pair was retained for further analysis if the following criteria were
379 met: 1) the PETH was significant in at least one bin within the 10–30 ms window (crossing both the
380 global and pointwise bands), and 2) the mode of the PETH was positive (the reader was activated after
381 the assembly).

382 Supralinearity of reader responses to assembly activations

383 To assess the supralinearity of reader responses to assembly activations, we first estimated the response
384 that could be expected from a hypothetical reader responding independently to individual assembly
385 members. To this end, we trained a generalized linear model (GLM) to predict the reader activity
386 around assembly member spikes outside of assembly activations:

$$R_{\Delta t}^{out} = W_{\Delta t} N^{out}$$

387 where N^{out} is a $(m + 1)$ -by- n^{out} matrix containing the spike counts of each of the m assembly members
388 (plus one constant term) in 15-ms bins around each of the n^{out} assembly member spikes outside assembly
389 activations, and $R_{\Delta t}^{out}$ is a 1-by- n^{out} vector containing the number of spikes of the reader neuron with
390 a delay Δt around each of the n^{out} spikes; $W_{\Delta t}$ is a 1-by- $(m + 1)$ vector containing the weights of the
391 GLM fit for delay Δt (Δt varies between -1 s and 1 s) to produce the curves in Fig. 2. This linear model
392 therefore captured the response of the reader at delay Δt if the reader were responding to each individual
393 assembly member independently. To estimate what the response of such a linear reader would be during
394 assembly activations, we computed:

$$\eta_{\Delta t} = w_{\Delta t} N^{in}$$

395 where N^{in} is a $(m + 1)$ -by- n^{in} matrix containing the spike counts of each of the m assembly members
396 (plus one constant term) in 15-ms bins around each of the n^{in} assembly member spikes emitted during
397 assembly activations, and $\eta_{\Delta t}$ is the activity predicted by the model for delay Δt . Thus, the *collective*
398 impact of the upstream assembly (beyond the sum of individual contributions) would be reflected in
399 reader responses beyond $\eta_{\Delta t}$. We quantified this supralinearity by computing:

$$S_{\Delta t} = \frac{R_{\Delta t}^{in} - \eta_{\Delta t}}{\eta_{20\text{ms}}}$$

400 where $R_{\Delta t}^{in}$ is a 1-by- n^{in} vector containing the number of spikes of the reader neuron with a delay Δt
401 around each of the n^{in} spikes, $\eta_{20\text{ms}}$ is a normalisation factor corresponding to the estimated linear
402 response $\eta_{\Delta t}$ at $\Delta t = 20$ ms, and $S_{\Delta t}$ is the reader supralinearity at delay Δt .

403 **Simulated readers** To estimate the supralinearity that would be expected from readers selective to
404 collective activity vs unresponsive to collective activity, we repeated the above analyses on simulated
405 data. We first simulated a ‘perfect’ reader that responded exclusively to the collective activity of the
406 assembly: it only fired 20 ms after each partial activation recruiting at least half of the largest subset of
407 co-active members (see *Pattern Completion* section below). We then simulated an ‘independent’ reader
408 which fired 20 ms after every spike emitted by an assembly member, regardless of any collective activity.

409 **Time scales** The above analysis used a time scale of 15-ms for cell assemblies (Fig. 2 and Fig. S5).
410 We repeated this analysis for multiple time scales (Fig. S7). Cell assemblies were detected as described
411 above, but using time bins of 1 ms, 5 ms, 10 ms, 15 ms, 20 ms, 25 ms, 30 ms, 40 ms, 50 ms, 75 ms, and
412 100 ms. One critical issue with this analysis is that larger time bins may contain assemblies expressed at
413 faster time scales: for instance, a 15-ms assembly also fits (and could thus also be detected) in time bins
414 of e.g. 30 ms or 100 ms — actually, in any time bin larger than 15 ms. To ensure that the analysis for
415 a given time scale only used assemblies specifically expressed at that time scale, we excluded all epochs
416 that contained activations of the same assembly at briefer time scales. The remaining activations were
417 used to split member spikes between n^{in} (assembly member spikes emitted during assembly activations)
418 and n^{out} (assembly member spikes emitted outside assembly activations). The two response curves (R^{in}
419 and η) were normalized conjointly: they were concatenated into a single vector for z-scoring.

420 Selectivity to identity of assembly members

421 To test whether the reader was sensitive to the co-activation of multiple assembly members, rather
422 than simply responding to the total spike output of assembly members, we compared the reader activity
423 around co-activations of two different assembly members ('AB') to the reader activity around the repeated
424 activation of a single assembly member ('AA').

425 For each assembly, we considered every possible permutation of two members. Each of these permutations
426 was analyzed independently, and from herein, the two neurons in a given permutation are termed 'A' and
427 'B'. To find 'AB' events, we performed a search in the inter-spike intervals of 'A' and 'B', retaining pairs
428 of spikes emitted by the two neurons within the assembly time scale (15 ms). To find a matching set of
429 'AA' events, we performed an equivalent search of moments when neuron 'A' emitted two consecutive
430 spikes within the same time scale (15 ms). Permutations in which we found less than 20 'AB' events or
431 less than 20 'AA' events were discarded from further analyses. We computed a peri-event time histogram
432 (PETH) of the firing rate of the reader neuron around 'AB' and 'AA' events, using the midpoint of
433 the two spikes ('AB' or 'AA') as a reference. The two PETHs were normalized conjointly: they were
434 concatenated into a single vector for z-scoring.

435 The above analysis used a time scale of 15-ms (Fig. S6). We repeated the analysis for multiple time scales
436 (Fig. 2, Fig. S8). Cell assemblies were detected as described above, but using bins of 1 ms, 5 ms, 10 ms,
437 15 ms, 20 ms, 25 ms, 30 ms, 40 ms, 50 ms, 75 ms, and 100 ms. For each time scale, we detected candidate
438 readers using the procedure outlined above. We further subdivided reader responses according to the
439 delay between the two spikes, within a precision of 5 ms. For example, to compute the reader response
440 to 'AA' events with a delay of 45 ms, we retained 'AA' events for which the two consecutive spikes were
441 within 42.5–47.5 ms of each other (without any 'A' or 'B' intervening spikes during this interval).

442 Pattern Completion

443 To quantify pattern completion, we determined the average reader responses to activation of all possible
444 combinations of assembly members. For example, for assembly 'ABCD', we measured reader responses to
445 the (complete) 4-member assembly activations 'ABCD', to each of the 3-member (incomplete) activations
446 'ABC', 'ABD', 'ACD', 'BCD', to each of the 2-member (incomplete) activations 'AB', 'AC', 'AD', 'BC',
447 'BD', 'CD', and to each of the single-member (incomplete) activations 'A', 'B', 'C', 'D', relative to the
448 baseline reader firing rate in all sleep periods. For each assembly–reader pair, we fit the resulting responses
449 with a sigmoid curve:

$$F_{\sigma}(x) = \frac{1}{1 + e^{-k(x-x_0)}}$$

450 where x is the proportion of active assembly members, and x_0 and k are the model parameters corre-
451 sponding to the midpoint and the steepness of the curve, respectively. To estimate the goodness-of-fit,
452 we computed

$$R_{\sigma}^2 = 1 - \frac{\sum_i (r_i - F_{\sigma}(n_i/n))^2}{\sum_i (r_i - \bar{r})^2}$$

453 where r_i is the reader response to combination i , and n_i/n is the proportion of active members. We
454 likewise estimated the goodness-of-fit of a proportional response $F_\alpha(x) = r_{complete} x$, where $r_{complete}$ is
455 the reader response to activations of the complete assembly (or of the largest subset of co-active members):

$$R_\alpha^2 = 1 - \frac{\sum_i (r_i - F_\alpha(n_i/n))^2}{\sum_i (r_i - \bar{r})^2}$$

456 Finally, we quantified the boost in observed response relative to the proportional response as the gain
457 $r - F_\alpha$. We split the data in tertiles according to x such that $x_1 \in (0, 1/3]$, $x_2 \in (1/3, 2/3]$, and $x_3 \in (2/3, 1]$
458 and tested each tertile for significant pattern completion.

459 Pattern Separation

460 To assess how readers discriminated between different assemblies, we first determined the response of
461 each neuron j following activations of each recorded assembly i , and computed the Hoyer coefficient of
462 sparsity:

$$H_j = \frac{\sqrt{n} - \frac{\sum_i^n r_{ij}}{\sqrt{\sum_i^n (r_{ij})^2}}}{\sqrt{n} - 1}$$

463 where n is the number of assemblies recorded simultaneously with neuron j , and r_{ij} is the response of
464 neuron j to assembly i . As neurons with lower baseline firing rates tend to have larger Hoyer coefficients
465 of sparsity, to compare across neurons we measured sparsity relative to surrogate data, where assembly
466 identities were shuffled across all pooled assembly activations (i.e., an activation of assembly a was
467 randomly assigned to assembly b). For each reader, we repeated this procedure 1000 times and computed
468 the mean Hoyer coefficient of the shuffled data H_j^0 . The sparsity increase relative to the shuffled data
469 was defined as:

$$H_j^{increase} = \frac{H_j - H_j^0}{H_j^0}$$

470 To determine whether reader responses were particularly sparse, we compared sparsity increases between
471 readers and non-readers (neurons for which a paired assembly could not be detected) using the Wilcoxon
472 rank sum test.

473 To test whether readers could discriminate between similar patterns, for each reader-assembly pair we
474 sought a second assembly with multiple overlapping members (at least 25% of each assembly and > 2 mem-
475 bers, e.g. ‘ABCD’ and ‘ABE’; varying the number of overlapping members did not change our results:
476 see Supplementary Figure 11), and defined the discrimination index between the two assemblies as:

$$d = \frac{r_1 - r_2}{r_1 + r_2}$$

477 where r_1 is the reader response to its paired assembly, and r_2 is its response to the overlapping assembly.
478 To test for significant discrimination, we computed discrimination indices for surrogate data, where the
479 activations of the two assemblies were pooled and the assembly identities were shuffled. This was repeated
480 1000 times, and when the discrimination index of a reader exceeded those of 95% of the shuffles, the reader
481 was considered to perform pattern separation.

482 Behavioral testing

483 Behavioral testing only relates to results shown in Fig. 4 as all other analyses were performed using data
484 from pre-training sleep sessions, i.e. preceding any exposure to the protocol described here.

485 The animals were tested in a slightly extended version of the standard fear conditioning and extinction
486 paradigm, initially intended to discriminate between cued and context fear learning. However, only

487 context extinction yielded useful data for the current study and is reported here. Briefly, fear conditioning
488 took place in one chamber (context), where foot shocks were associated with auditory stimuli (conditioned
489 stimuli, CS). Extinction took place either in the same chamber without the CS (contextual extinction),
490 or in a different chamber with the CS (cued extinction). Daily recording sessions consisted of two 37-min
491 exposure sessions (one per chamber), preceded, separated, and followed by sleep sessions of 2-3 hours.
492 Only sleep periods before and after exposure to the conditioning chamber were analyzed here, amounting
493 to two pre-training control sessions, two fear conditioning sessions, and two extinction sessions per animal.

494 The conditioning chamber was cubic (side length, 40 cm) with gray plexiglass walls lined with ribbed
495 black rubber sheets and a floor composed of nineteen stainless steel rods (0.48 cm diameter, 1.6 cm
496 spacing) connected to a scrambled shock generator (ENV-414S, Med Associates, USA). It was mildly
497 scented daily with mint-perfumed cleaning solution (Simple Green, Sunshine Makers). A custom-made
498 electronic system presented the animals with two auditory CS (80 dB, 20 s long, each composed of 1 Hz,
499 250 ms long pips of either white noise, CS+ paired to shocks, or 8 kHz pure tones, CS- unpaired). These
500 auditory stimuli (8 CS+ and 8 CS-) were presented starting at $t = 3$ min, separated by random-duration
501 inter-trial intervals (120–240 s). Foot shocks consisted in shocks scrambled across floor rods (1 s, 0.6 mA,
502 co-terminating with CS+ presentations; CS+ and CS- were presented in pseudorandom order allowing no
503 more than 2 consecutive presentations of the same-type CS). Sleep was recorded in a cloth-lined plastic
504 flowerpot (30 cm upper diameter, 20 cm lower diameter, 40 cm high).

505 **Data availability**

506 The datasets generated during the current study are available in the [NAME] repository [LINK WILL
507 BE PROVIDED UPON ACCEPTATION].

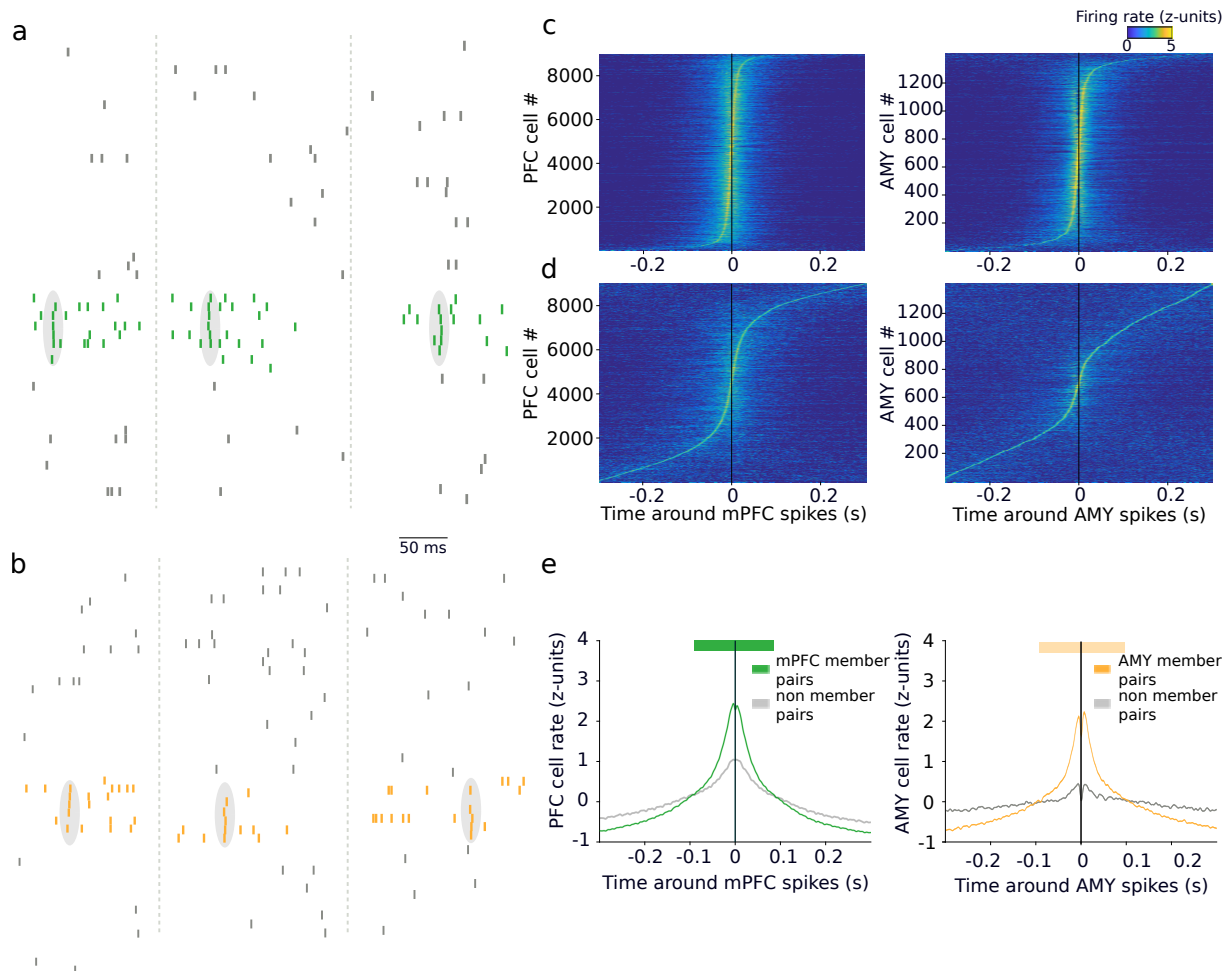


Fig. S1. Cell assemblies in the cortico-amygdalar circuit. **a**, Spike trains of a subset of 35 simultaneously recorded units in prefrontal cortex during sleep (rasters: action potentials; gray ellipses surrounding colored ticks: co-activation events). **b**, Spike trains of a subset of 30 simultaneously recorded units in the amygdala during sleep (rasters: action potentials; gray ellipses surrounding colored ticks: co-activation events). **c**, Z-scored cross-correlations between members of the same prefrontal (left) and amygdalar (right) assemblies, ordered by mode. **d**, Same as in (c) for control pairs, illustrating that fewer pairs have modes at brief delays. **e**, Averages of (c) (colored curves) and (d) (gray curves). Members of the same assemblies had significantly higher synchrony at short delays than control pairs (thick horizontal colored bars: $p < 0.05$, Monte-Carlo bootstraps).

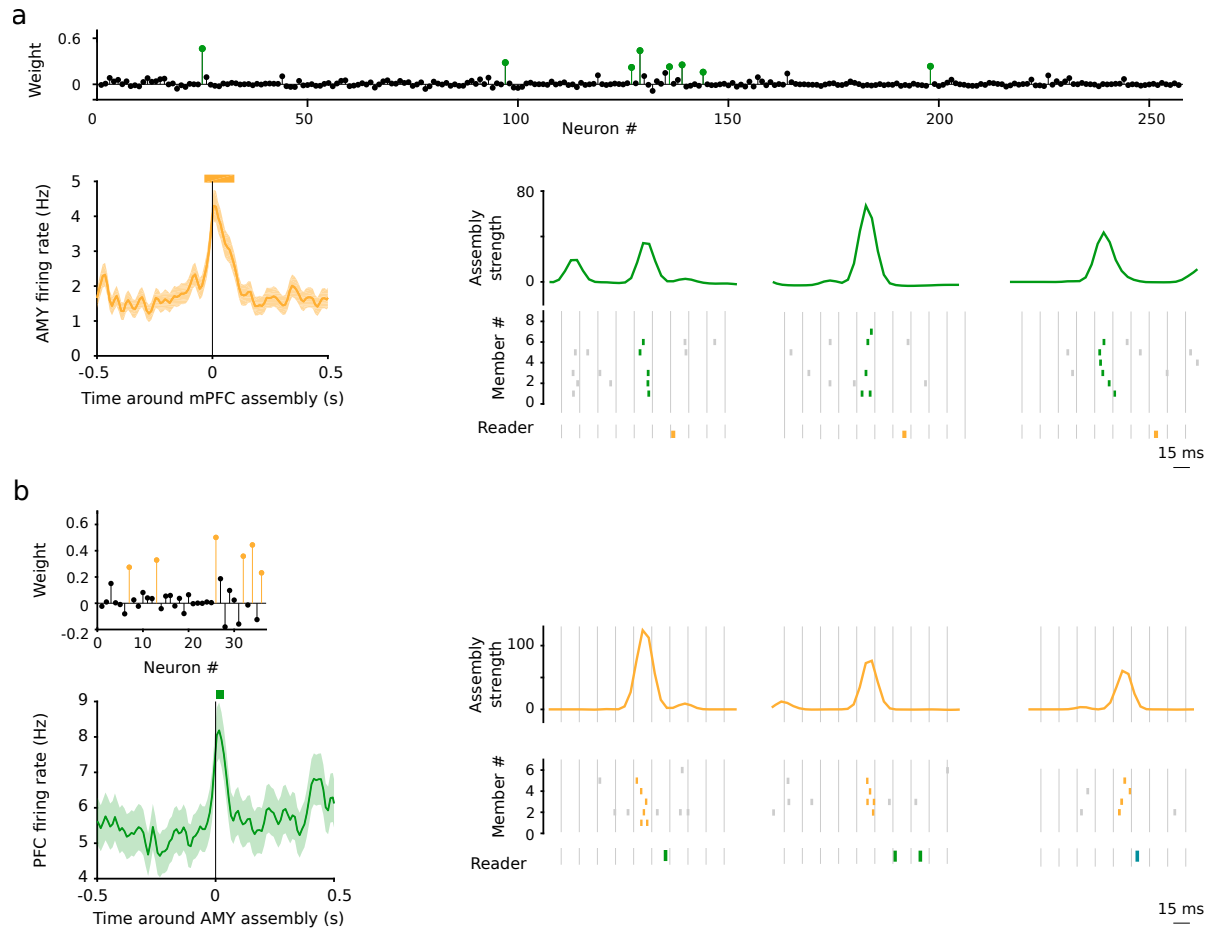


Fig. S2. Example assembly–reader pairs. **a**, Activations of a prefrontal assembly closely followed (10–30 ms) by significant responses of an amygdalar neuron. Top: cell assembly weights (colored circles: assembly members, black circles: non-members). Bottom left: firing rate of an amygdalar neuron centered on all prefrontal assembly activations (mean \pm s.e.m.). Thick orange horizontal bar indicates significant responses ($p < 0.05$: Monte-Carlo bootstrap test; see Methods). Bottom right: example assembly activations (green curves: activation strength) followed by downstream spiking (rasters: prefrontal spikes within (green) or outside (gray) epochs of assembly activation; orange rasters: amygdalar spikes). Reader responses occurred ~ 20 ms after assembly activations. **b**, Same as (a) for an amygdalar assembly and a downstream prefrontal neuron.

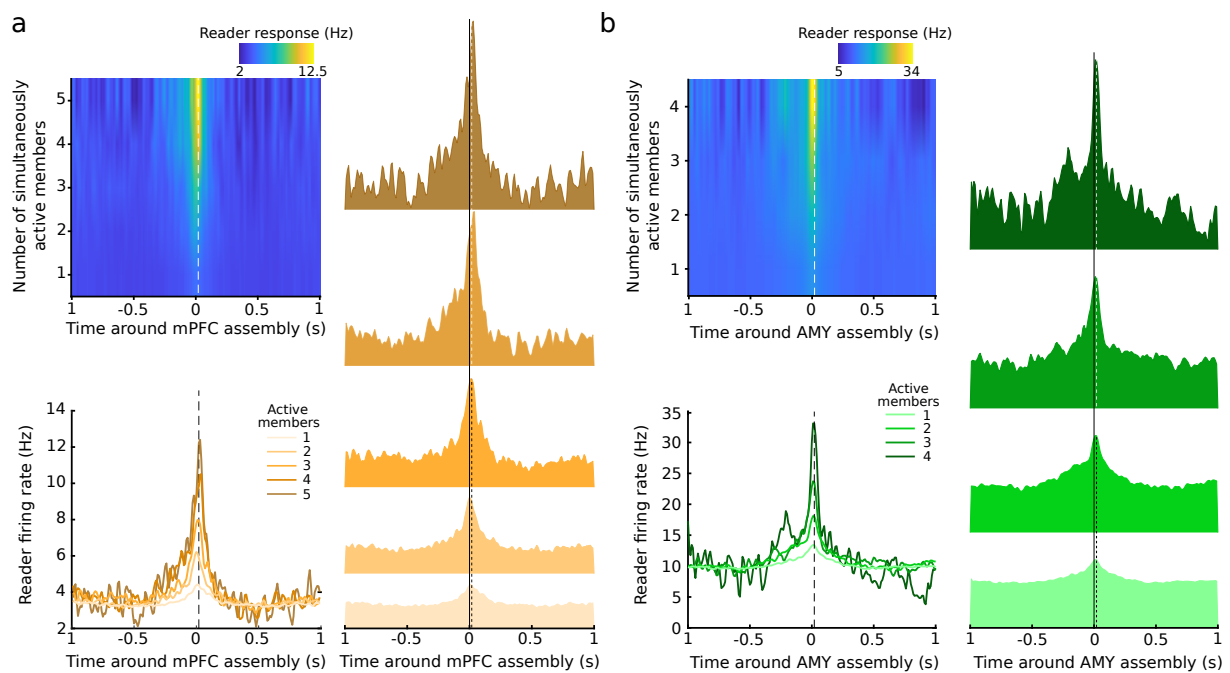


Fig. S3. Assembly members exert a synergistic influence on their targets: reader response rate increases with the number of co-active assembly members. **a**, Example amygdalar response to increasing numbers of simultaneously active prefrontal assembly members. Top left: Reader firing rate centered on assembly activation. Right: Reader firing rate for different numbers of co-active members. Bottom left: Superimposed response curves. **b**, Same as (a) for example prefrontal assembly and amygdalar reader.

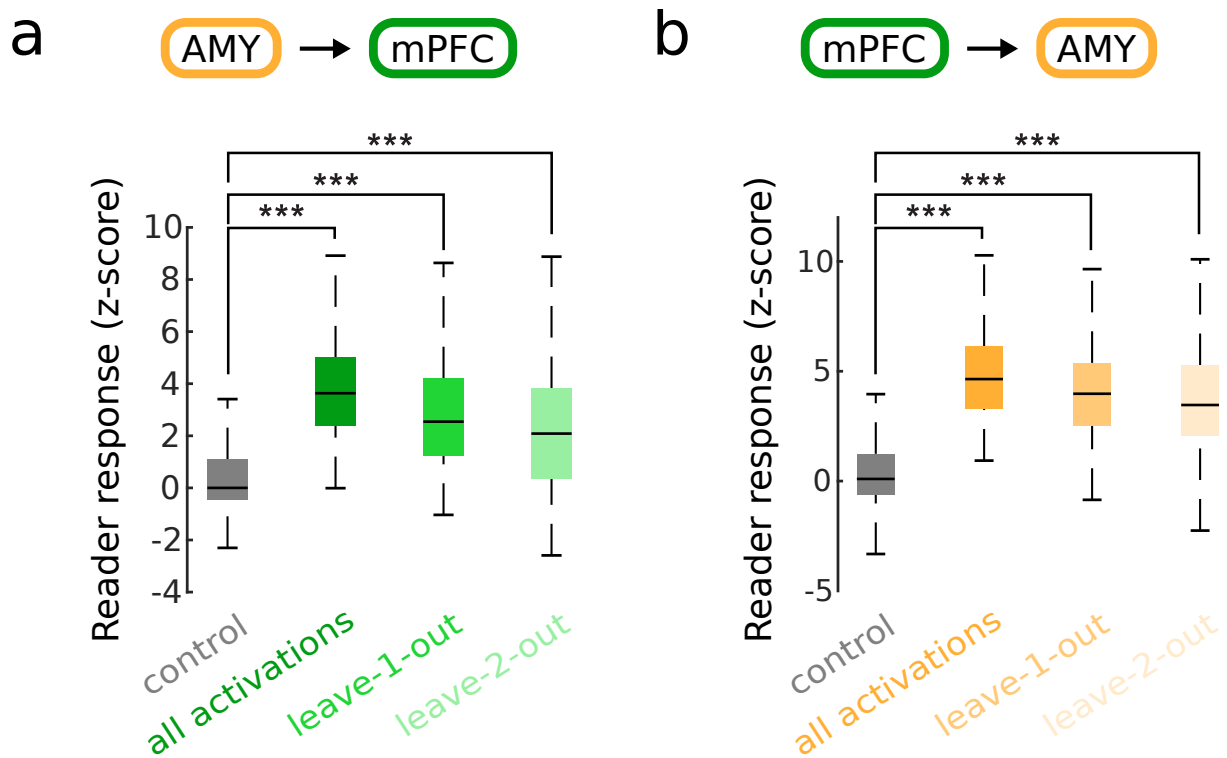


Fig. S4. Assembly members exert a synergistic influence on their targets: responses are not driven by single ‘vocal’ members. **a**, Average response of prefrontal readers to amygdalar assembly activations when the most effective members (i.e. the members whose spikes outside assembly activation epochs were followed by the largest response by the reader neuron at 10–30 ms) of upstream assemblies were not recruited (leave 1-out, leave 2-out). **b**, Same as **(a)** for amygdalar reader responses to member spikes of prefrontal assemblies.

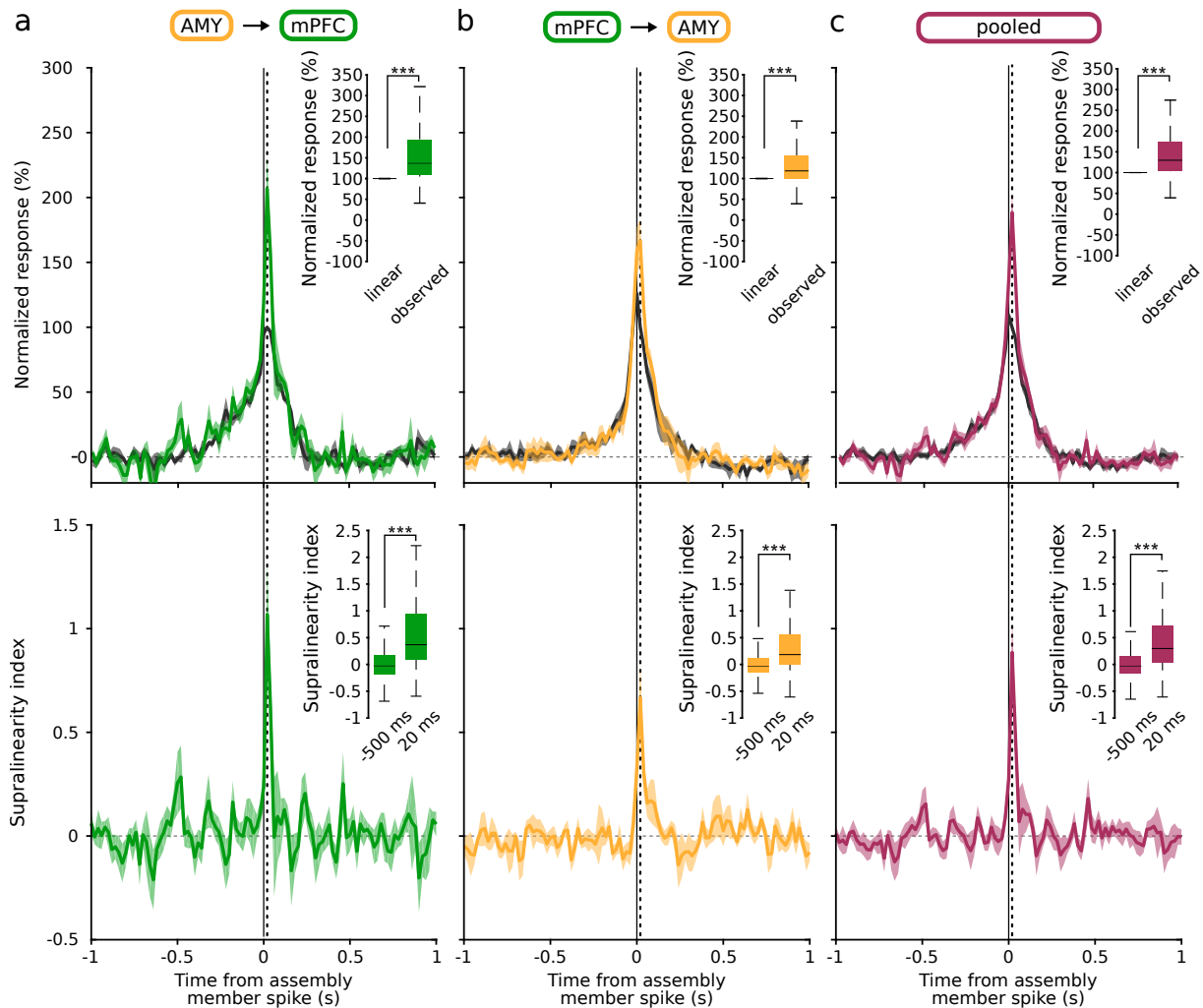


Fig. S5. Supralinearity of reader responses. **a**, Top: Observed responses (colored curve: mean \pm s.e.m.) of prefrontal readers compared to the estimated response of a linear reader (gray curve: mean \pm s.e.m.). Inset: The observed response was greater than the linear estimate at 20 ms ($***p < 0.001$, Wilcoxon signed-rank test). Bottom: Supralinearity index of prefrontal reader responses. Dashed line: peak of reader responses to assembly activations at 20 ms. Inset: Supralinearity at 20 ms vs baseline ($***p < 0.001$, Wilcoxon signed-rank test). **b**, Same as (a) for amygdalar reader responses to spikes of members of prefrontal assemblies. **c**, Same as (a) for pooled responses of both amygdalar and prefrontal readers.

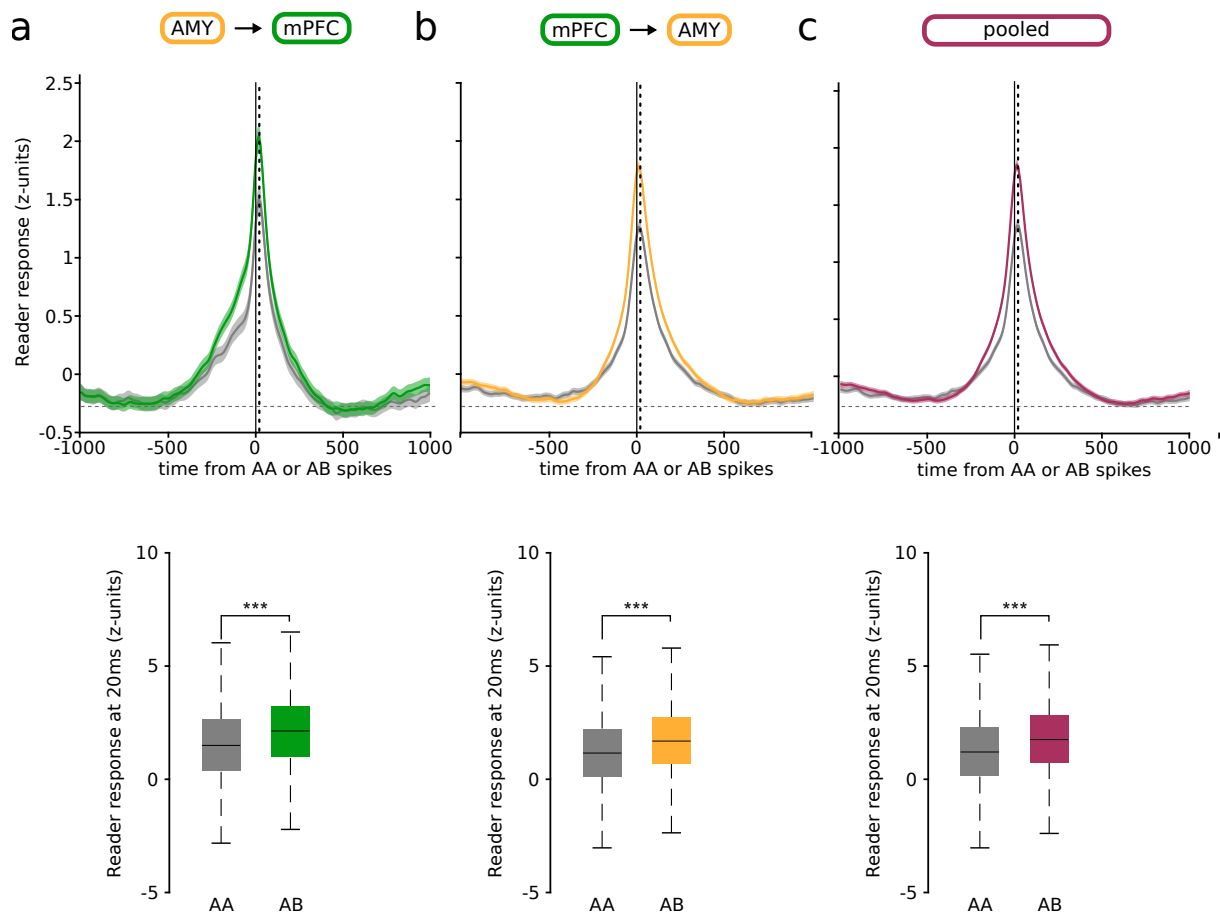


Fig. S6. The identity of participating members matters beyond their compound activity. **a**, Response of prefrontal readers to amygdalar assembly members. Top: z-scored responses of reader neurons to two spikes emitted by different assembly members (AB, colored curve), compared to the control responses to two spikes emitted by the same assembly member (AA, gray curve) (mean \pm sem). Bottom: Z-scored reader responses at 20 ms (** $p < 0.001$, Wilcoxon signed-rank test). **b**, Same as (a) for amygdalar readers and PFC assembly members. **c**, Same as (a) for pooled responses of both amygdalar and prefrontal readers.

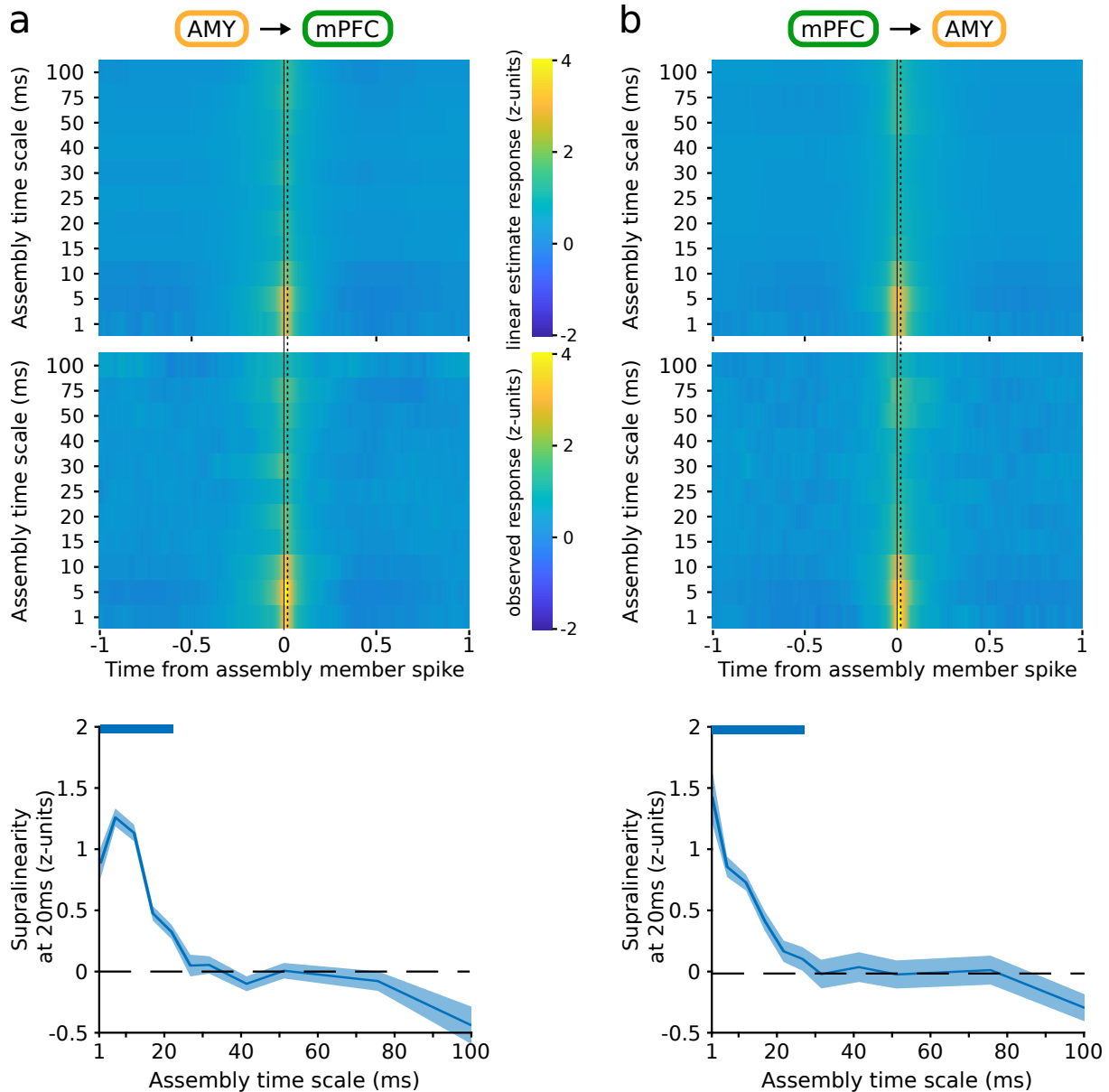


Fig. S7. Time scale of reader response supralinearity. **a**, Response of prefrontal readers to activations of amygdalar assemblies at varying time scales. Top and center: mean z-scored responses of a linear model vs the observed reader response, as a function of the time scale of the assembly. Bottom: difference between the two (observed response–linear estimate), for varying time scales. Thick colored horizontal bars indicate significant differences ($p < 0.05$, Monte-Carlo bootstrap test). **b**, Same as **(a)** for amygdalar reader responses to member spikes of prefrontal assemblies. Note that in both cases, supralinearity is significantly greater than 0 for time scales up to 20–25 ms.

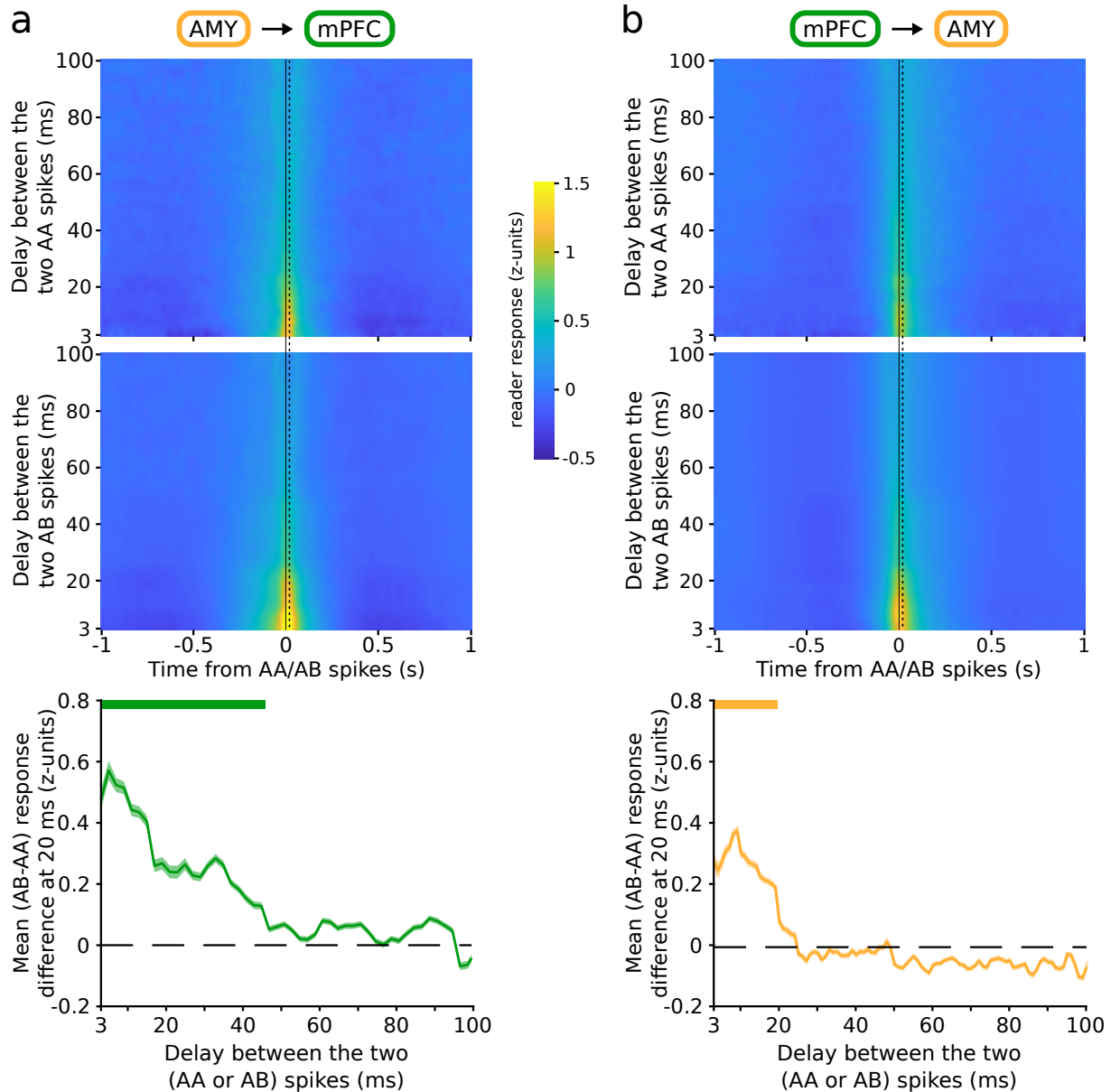


Fig. S8. Time scale of reader sensitivity to assembly member identity. **a**, Response of prefrontal readers to two spikes emitted by different assembly members (AB), compared to the control responses to two spikes emitted by the same assembly member (AA), at varying time scales. Top and center: mean z-scored responses of reader neurons to spikes emitted by the same (AA, top) vs different (AB, center) members of an upstream assembly, as a function of the temporal delay between the two spikes. Bottom: difference between the two (AB–AA), for varying temporal delays. Thick colored horizontal bars indicate significant difference ($p < 0.05$, Monte-Carlo bootstrap test). **b**, Same as (a) for amygdalar readers.

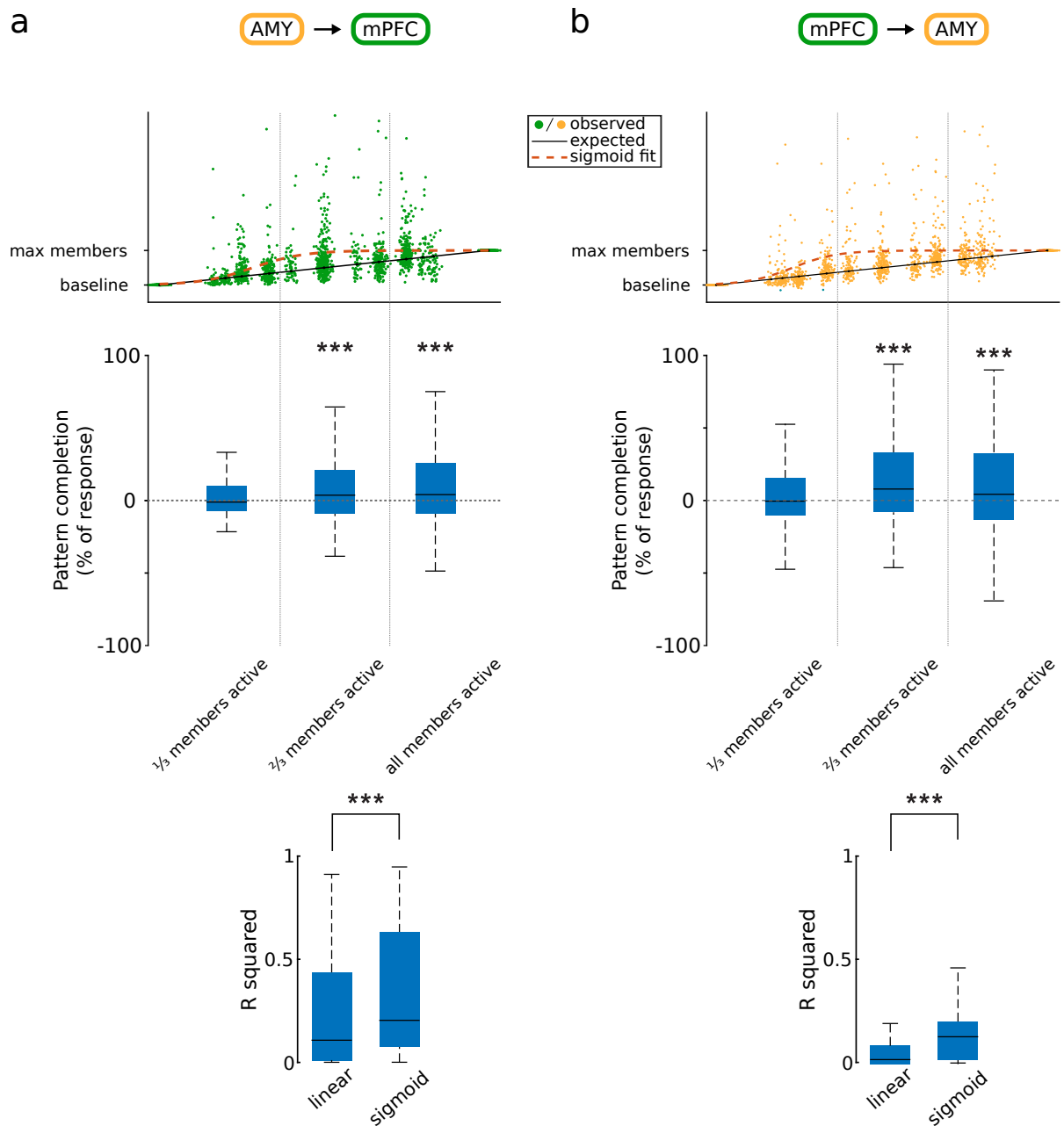


Fig. S9. The assembly–reader mechanism can implement pattern completion. **a**, Prefrontal reader responses to amygdalar assemblies. Top: Pooled reader responses as a function of the proportion of active assembly members. Black line: linear response. Dashed red curve: best-fit sigmoid curve. Center: boost in reader response (relative to a proportional response) for all assembly–reader pairs as a function of the proportion of active assembly members. The gain was significant for the second and third quantiles ($***p < 0.001$, Wilcoxon signed-rank test), but not for the first quantile ($*p < 0.05$, Wilcoxon signed-rank test). Bottom: The data were better fit with sigmoidal than linear models ($***p < 0.001$, Wilcoxon signed-rank test). **b**, Same as **(a)** for amygdalar reader responses to prefrontal assemblies.

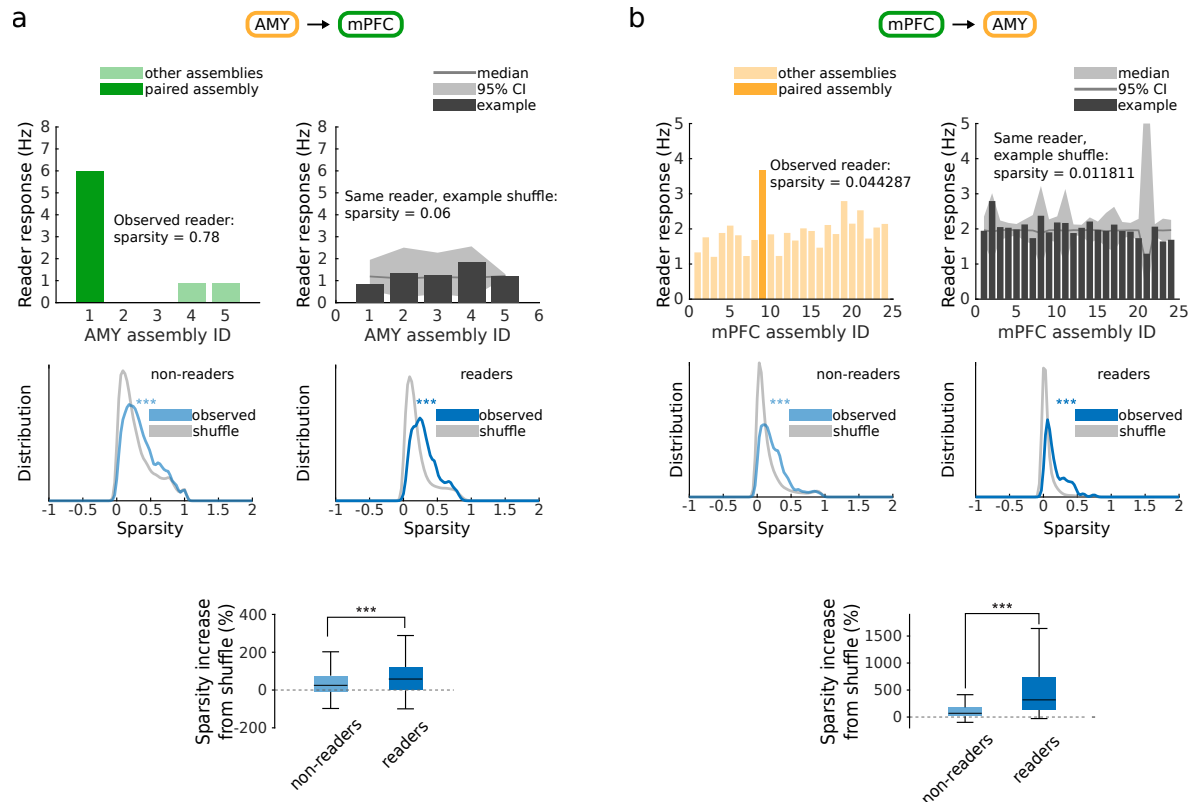


Fig. S10. The assembly–reader mechanism can implement pattern separation: reader responses are selective for specific assemblies. **a**, Sparsity of prefrontal reader responses to amygdalar assemblies. Top left: Responses of an example prefrontal neuron to each amygdalar cell assembly in the recording session. Responses are selective for the paired assembly (dark green), compared to other assemblies (light green). Top right: Control responses of the same prefrontal neuron to surrogate assembly activations (shuffled assembly identities) are not selective. Center: distribution of sparsity for non-reader (left) and reader (right) neurons, compared to control sparsity computed from shuffled data (gray). Note that the observed responses are sparser than the shuffled control ($***p < 0.001$, Wilcoxon signed rank test). Bottom: Sparsity increase from shuffle, for reader vs non-reader neurons ($***p < 0.001$, Wilcoxon rank sum test). **b**, Same as (**a**) for amygdalar reader responses to prefrontal assemblies.

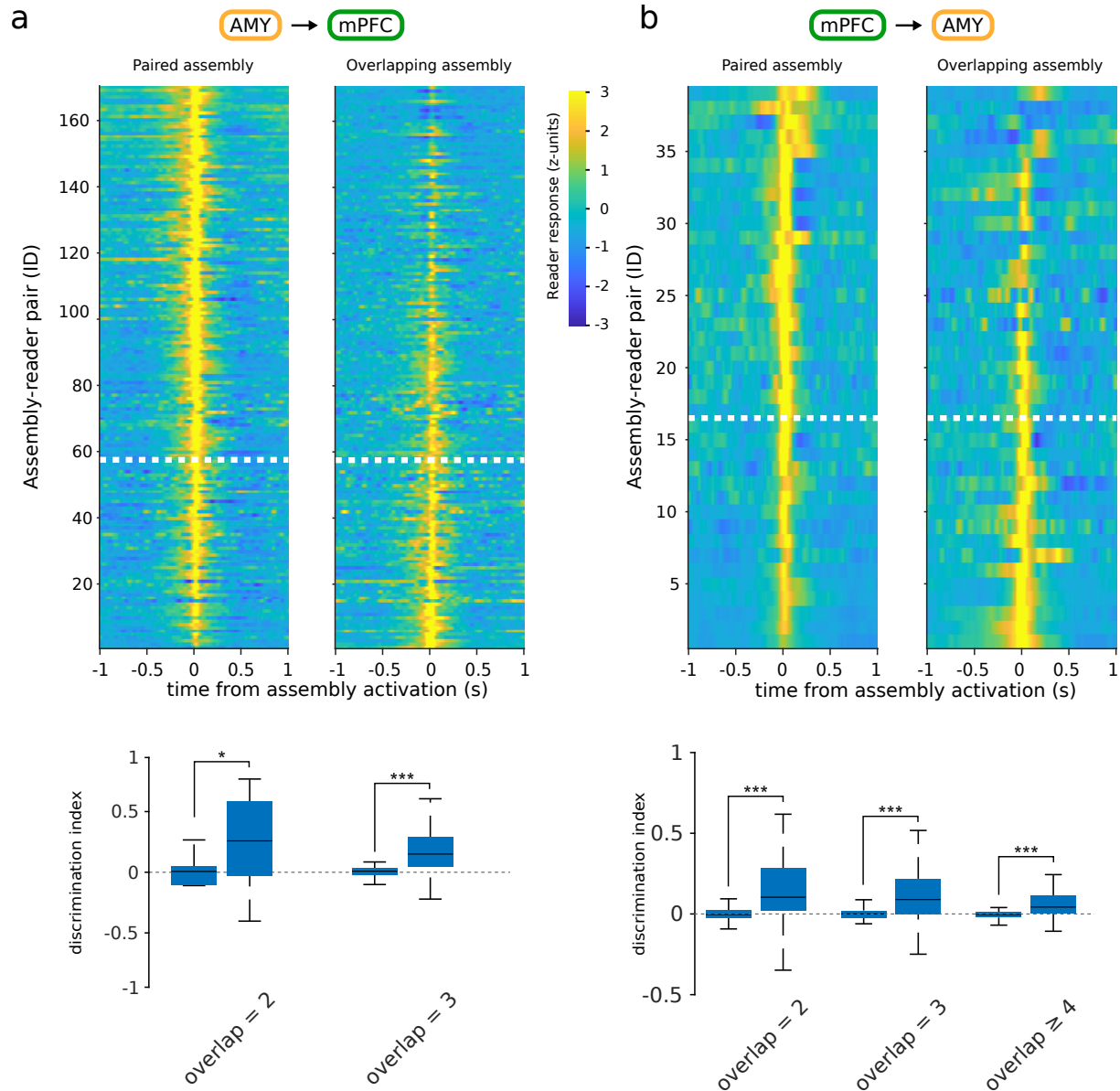


Fig. S11. The assembly–reader mechanism can implement pattern separation: readers can discriminate between overlapping assemblies. **a**, Pattern separation in prefrontal reader responses to amygdalar assemblies. Top: prefrontal reader responses to activation of a paired assembly (left) vs a different but overlapping ($\geq 25\%$) assembly, sorted by discrimination index. Responses above the white dotted line manifested significant pattern separation (greater discrimination indices than shuffled data, $p < 0.05$, Wilcoxon rank sum test). Bottom: Discrimination indices were greater for observed than shuffled data ($***p < 0.001$, Wilcoxon rank sum test). **b**, Same as (a) for amygdalar reader responses to prefrontal assemblies.

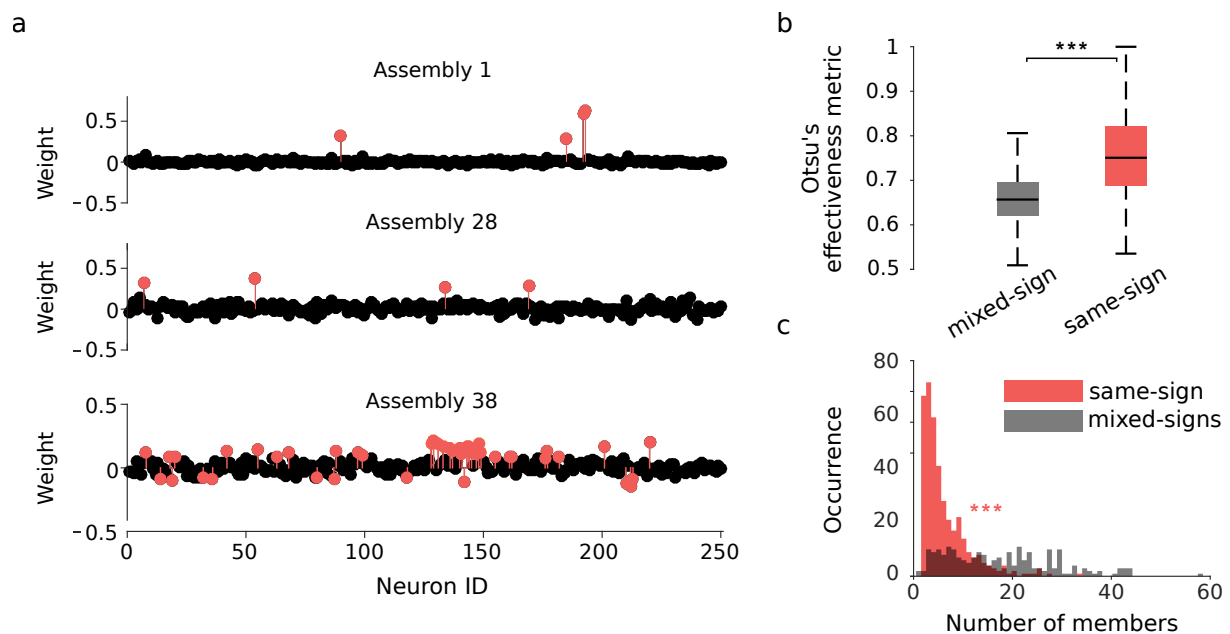


Fig. S12. Selection of cell assemblies with same-sign component weights. **a**, Cell assembly weights of three representative prefrontal assemblies (colored circles: assembly members, black circles: non-members), corresponding to eigenvalues 1, 28 and 38. Whereas all members of assemblies 1 and 28 were of the same (positive) sign, assembly 38 included members with both positive and negative weights ('mixed-sign assembly'). **b**, The separation between members and non-members was significantly better in same-sign assemblies than mixed-sign assemblies ($***p < 0.001$, Wilcoxon rank sum test). **c**, Mixed-sign assemblies had significantly more members than same-sign assemblies ($***p < 0.001$, Wilcoxon rank sum test).

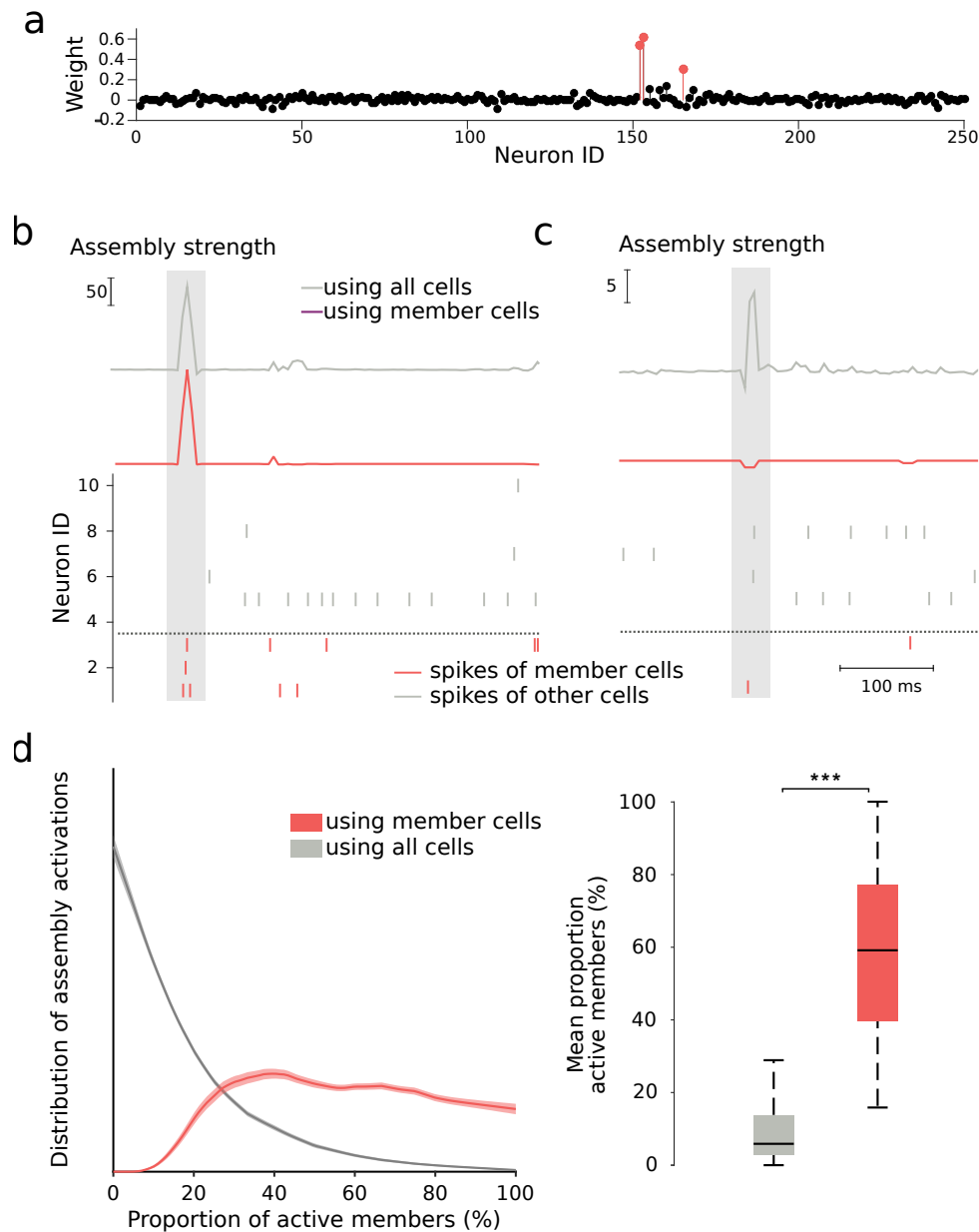


Fig. S13. Computation of assembly activation strength. **a**, An example assembly recorded in the prefrontal cortex. Red dots: assembly members. **b**, Example activation of assembly shown in **(a)**. Top: Assembly activation strength computed using either the activity of all cells (gray curve) or the activity of member cells only (red curve). Bottom: Raster plot of the activity of a representative subset of neurons, ordered by absolute weight (vertical ticks: action potentials; red ticks: member cells; gray ticks: non-member cells; shaded rectangle: putative assembly activation). All three members were active, resulting in a high activation strength in both curves. **c**, Same as **(b)** but for an instance in which only a single assembly member was active, at the same time as two non-members. The corresponding peak in the gray curve would result in incorrect detection of an activation of the assembly. This spurious peak is absent from the red curve, where activity strength is computed using only assembly members. **d**, Left: Proportion of assembly members co-active around peaks in the assembly activation strength computed using the activity of member cells only (red) or using the activity of all cells (gray). Right: using the activity of member cells results in detection of assembly activation events with greater proportions of co-active members ($***p < 0.001$, Wilcoxon signed rank test).

Figure	Test	Description	P-value	N	Effect size
1.b (left)	Wilcoxon rank sum test	GLM gain (%) vs shuffled data (PFC)	$p = 0$	2061	∞
1.b (right)	Wilcoxon rank sum test	GLM gain (%) vs shuffled data (AMY)	$p = 1.767 \cdot 10^{-202}$	676	30,3
1.f (top)	Wilcoxon signed-rank test	% of assembly-reader pairs vs chance	$p = 6.1 \cdot 10^{-5}$	20	4
1.f (bottom)	Wilcoxon signed-rank test	% of assembly-reader pairs vs chance	$p = 1.2 \cdot 10^{-4}$	20	3,84
2.a	Wilcoxon rank sum test	reader neuron responses (all activations) vs control	$p = 0$	849	∞
2.a	Wilcoxon rank sum test	reader neuron responses (leave-1-out) vs control	$p = 1.1887 \cdot 10^{-320}$	849	38,2827
2.a	Wilcoxon rank sum test	reader neuron responses (leave-1-out) vs control	$p = 2.0842 \cdot 10^{-196}$	849	29,8981
2.b	Wilcoxon signed-rank test, one-tailed	supralinearity index (observed data) vs baseline	$p = 1.336 \cdot 10^{-98}$	1173	$z = 21.043$
2.b	Wilcoxon signed-rank test, one-tailed	supralinearity index (perfect reader) vs baseline	$p = 8.416 \cdot 10^{-169}$	1173	$z = 27.668$
2.b	Wilcoxon signed-rank test, one-tailed	supralinearity index (independent reader) vs baseline	$p = 0.7916$	1173	$z = -0.812$
2.c	Wilcoxon signed-rank test, one-tailed	response to AA events vs AB events (5 ms delay)	$p = 1.840 \cdot 10^{-91}$	4443	$z = 20.248$
2.c	Wilcoxon signed-rank test, one-tailed	response to AA events vs AB events (10 ms delay)	$p = 3.088 \cdot 10^{-87}$	6520	$z = 19.763$
2.c	Wilcoxon signed-rank test, one-tailed	response to AA events vs AB events (15 ms delay)	$p = 3.072 \cdot 10^{-121}$	10288	$z = 23.384$
2.c	Wilcoxon signed-rank test, one-tailed	response to AA events vs AB events (20 ms delay)	$p = 2.490 \cdot 10^{-77}$	8487	$z = 18.576$

2.c	Wilcoxon signed-rank test, one-tailed	response to AA events vs AB events (25 ms delay)	$p = 0.1315$	12056	$z = 1.119$
2.c	Wilcoxon signed-rank test, one-tailed	response to AA events vs AB events (50 ms delay)	$p = 1$	10383	$z = -9.900$
2.c	Wilcoxon signed-rank test, one-tailed	response to AA events vs AB events (100 ms delay)	$p = 0.9996$	8166	$z = -3.415$
line 102	chi-square test	amygdalar readers vs non-readers likeliness to participate in cell assemblies targeting prefrontal readers	$p = 1.2 \cdot 10^{-4}$	204, 920	odds ratio: 2.943
line 107	chi-square test	prefrontal readers vs non-readers likeliness to participate in cell assemblies targeting amugdalar readers	$p = 2.6 \cdot 10^{-21}$	404, 2018	odds ratio: 1.797
3.a center	Sign test, one-tailed	reader response vs proportional response to co-activation of up to one third of members	$p = 0.7186$	967	$z = -0.579$
3.a center	Sign test, one-tailed	reader response vs proportional response to co-activation of more than one third and up to two thirds of members	$p = 1.3748 \cdot 10^{-13}$	1247	$z = 7.306$
3.a center	Sign test, one-tailed	reader response vs proportional response to co-activation of more than two thirds of members (but not all members)	$p = 0.7186$	613	$z = 3.312$
3.a bottom	Wilcoxon signed-rank test	linear vs sigmoidal fit	$p = 2.844 \cdot 10^{-132}$	1026	$z = -24.473$
3.b bottom	Wilcoxon rank sum test	sparsity increase non-readers vs readers	$p = 2.5792 \cdot 10^{-12}$	2018, 404	$z = -6.999$
3.c	Wilcoxon rank sum test	Discrimination indices observed vs shuffled data	$p = 3.9281 \cdot 10^{-27}$	100, 10000	$z = 10.788$

4.b	chi-square test	proportion of AMY-PFC assembly–reader pairs significantly changed their responses following fear conditioning vs following control sessions	$p = 0.0017$	171, 260	odds ratio: 1.677
4.b	chi-square test	proportion of AMY-PFC assembly–reader pairs significantly changed their responses following fear extinction vs following control sessions	$p = 0.7253$	235, 260	odds ratio: 1.106
4.b	chi-square test	proportion of PFC-AMY assembly–reader pairs significantly changed their responses following fear conditioning vs following control sessions	$p = 0.1403$	171, 267	odds ratio: 1.582
4.d	chi-square test	proportion of PFC-AMY assembly–reader pairs significantly changed their responses following fear extinction vs following control sessions	$p = 0.0347$	123, 267	odds ratio: 2.060

Table S1: Detailed Statistics